


8-2019

# Evaluation of the METRIC model for mapping energy balance components and actual evapotranspiration for a super-intensive drip-irrigated olive orchard

Samuel Ortega

University of Nebraska - Lincoln, sortegas88@hotmail.com

Follow this and additional works at: <https://digitalcommons.unl.edu/natresdiss>

 Part of the [Hydrology Commons](#), [Natural Resources and Conservation Commons](#), [Natural Resources Management and Policy Commons](#), [Other Environmental Sciences Commons](#), and the [Water Resource Management Commons](#)

---

Ortega, Samuel, "Evaluation of the METRIC model for mapping energy balance components and actual evapotranspiration for a super-intensive drip-irrigated olive orchard" (2019). *Dissertations & Theses in Natural Resources*. 296.

<https://digitalcommons.unl.edu/natresdiss/296>

This Article is brought to you for free and open access by the Natural Resources, School of at DigitalCommons@University of Nebraska - Lincoln. It has been accepted for inclusion in Dissertations & Theses in Natural Resources by an authorized administrator of DigitalCommons@University of Nebraska - Lincoln.

Evaluation of the METRIC model for mapping energy balance components and actual  
evapotranspiration for a super-intensive drip-irrigated olive orchard

by

Samuel Ortega-Salazar

A THESIS

Presented to the Faculty of  
The Graduate College at the University of Nebraska  
In Partial Fulfillment of Requirements  
For the Degree of Master of Science

Major: Natural Resource Sciences

Under the Supervision of Professor Ayse Kilic  
Lincoln, Nebraska

August, 2019

Evaluation of METRIC model for mapping energy balance components and actual evapotranspiration of a super-intensive drip-irrigated olive orchard

Samuel Ortega-Salazar, M.S.

University of Nebraska, 2019

Advisor: Ayse Kilic

A field experiment was carried out to evaluate the METRIC (Mapping EvapoTranspiration at high Resolution Internalized with Calibration) model for mapping net radiation ( $R_{ni}$ ), soil heat flux ( $G_i$ ), sensible heat flux ( $H_i$ ), latent heat flux ( $LE_i$ ), actual evapotranspiration ( $ET_a$ ) and crop coefficient ( $K_c$ ) of a superintensive drip-irrigated olive (*Olea europae* L. cv Arbequina) orchard located in Penciahue Valley, Region del Maule, Chile (35° 23' LS; 71° 44' LW; 96 m above sea level). The study was conducted in an experimental plot of 21.1 hectares using 9 satellite images (Landsat 7 ETM+) acquired on clear sky days during 2011/2012 and 2012/2013 growing seasons. Specific functions to estimate  $G_i$ , leaf area index (LAI) and aerodynamic roughness length for momentum transfer ( $z_{om}$ ) were incorporated in the standard METRIC model. The performance of the METRIC model was evaluated at the time of satellite overpass using measurements of LE and H obtained from an eddy correlation system. Validation indicated that METRIC using the specific functions was able to estimate  $R_n$ , G, H, LE,  $ET_a$ , and  $K_c$  with errors less than +5%.

## CHAPTER 1 INTRODUCTION

In Chile, the olive oil industry has significantly increased during the last decade, especially in semi-arid Mediterranean regions which present hot and dry summer climate associated with very low precipitation ( $< 50$  mm) during growing seasons. In these regions, the new plantations have included the drip-irrigation and super-intensive training systems with plant density ( $> 1000$  trees  $\text{ha}^{-1}$ ) (López-Olivari et al., 2015). However, the stability and growth of the olive oil industry will be significantly affected by future scenarios of water scarcity. Under these conditions, the orchard irrigation management will be the key to maintaining the yield and quality of the olive oil production (Ahumada-Orellana et al., 2018, 2017). For an optimum irrigation management, it is crucial to estimate the orchard water requirements or actual evapotranspiration (ETa) according to the spatial variability of soil, cultivar and climate (López-Olivari et al., 2016; Ortega-Farias et al., 2009). Traditionally, ETa is quantified using a grass or alfalfa reference evapotranspiration ( $\text{ET}_{\text{r}24}$ ) at 24 hours and single crop coefficient ( $K_c$ ). Also, it has been suggested using the dual crop coefficient approach to describe the ratio of ETa to  $\text{ET}_{\text{r}24}$  by separating  $K_c$  into basal crop coefficient ( $K_{cb}$ ) and soil evaporation coefficient ( $K_e$ ) (Er-Raki et al., 2010). For heteronomous canopies such as olive orchards, however, values of  $K_c$  and  $K_{cb}$  require local adjustment because they depend on canopy architecture and non-linear interaction of soil, cultivar, and climate (Cammalleri et al., 2013; Ortega-Farias et al., 2009; Paço et al., 2014). Also, López-Olivari et al., (2016) indicated that water consumption in super-intensive olive orchards is dominated by the canopy cover which is generally non-uniform as a result of the tree geometry generated by training systems. In this case, the energy absorbed by the vegetation and also by the

soil surface rely on the spatial variability of canopy size, soil characteristics, leaf area index (LAI), and fractional cover (fc). For this reason, it is necessary to incorporate methodologies that can take into account the effect of the intra-orchard spatial variability of soil and tree vigor on the estimation of Kc and ETa.

In recent decades, remote sensing energy balance (RSEB) techniques have become a valuable tool to evaluate the spatiotemporal variability of energy balance components, ETa and Kc for complex canopy structures like orchards (Cammalleri et al., 2013; de la Fuente-Sáiz et al., 2017; He et al., 2017; Jin et al., 2018; Pôças et al., 2014; Ramírez-Cuesta et al., 2019). The RSEB models estimate the ETa for each pixel of a satellite image as a “residual” component of the orchard energy balance at the time of satellite overpass:

$$LE_i = \lambda \cdot ETa_i = Rn_i - G_i - H_i \quad (\text{Eq. 1.1})$$

where  $LE_i$  is the latent heat flux ( $W m^{-2}$ ),  $Rn_i$  is net radiation ( $W m^{-2}$ ),  $ETa_i$  is actual evapotranspiration ( $mm h^{-1}$ ),  $G_i$  is soil heat flux ( $W m^{-2}$ ),  $H_i$  is the sensible heat flux ( $W m^{-2}$ ) and  $\lambda$  is the latent heat of vaporization ( $J Kg^{-1}$ ). Subscript “i” indicates instantaneous values.

The METRIC (Mapping EvapoTranspiration at high Resolution using Internalised Calibration) model has been recently applied to evaluate the spatial variability of ETa and Kc of orchards with promising results (de la Fuente et al., 2017; He et al., 2017; Jin et al., 2018; 2014; Pôças et al., 2014; Paço et al 2014). METRIC uses an internal self-calibration (Inverse Modeling at Extreme Conditions, CIMEC) to remove effects of biases in atmospheric correction of reflectance, surface temperature and estimation of  $H_i$

(Allen et al., 2007, 2011). In addition, the internal self-calibration of METRIC calibrates the sensible heat flux using two extreme conditions (hot pixel and cold pixel) or “anchor pixels”. However, Allen et al., (2011) indicate that the main limitation of METRIC is that the quantification of  $LE_i$  for each pixel is only as accurate as the estimates for  $Rn_i$ ,  $G_i$  and  $H$ .

It is acknowledged that originally the METRIC model was developed for annual crops, and it might not apply as accurately to sparse crops such as super-intensive olive orchards with low fractional cover and heterogeneous canopy. In this regard, several researchers have suggested that the adjustment of some intermediate parameters in the standard METRIC, such as the momentum roughness length ( $z_{om}$ ), LAI and  $G_i$  can reduce the uncertainties of  $LE_i$  and  $ETa_i$  estimates for heterogeneous woody canopies such as orchards and vineyards (Carrasco-Benavides et al., 2014; de la Fuente-Sáiz et al., 2017; Jin et al., 2018; Pôças et al., 2014; Santos et al., 2012). For a non-irrigated olive orchard, Santos et al. (2012) found that the METRIC-based  $ETa$  estimates were improved using the Perrier roughness function to compute  $z_{om}$  (RMSE was reduced from 1.12 to 0.25  $mm \cdot d^{-1}$ ). For a commercial super-intensive olive orchard, Pôças et al. (2014) indicated that METRIC performance showed a quantitative improvement of  $ETa$  estimates when applying three-source conditions for temperature estimation, as well as the  $z_{om}$  computation with the Perrier equation. For a drip-irrigated apple orchard, de la Fuente et al. (2017) found that METRIC using the calibrated functions estimated  $H_i$  and  $LE_i$  with errors of 5 and 16%, while using the original functions estimated  $H_i$  and  $LE_i$  with error of 29 and 26%, respectively. Finally, for micro-irrigated pistachio orchards, Jin et al. (2018) observed that recalibrated METRIC was able to simulate  $ETa$  with

MAE = 1.1 mm d<sup>-1</sup> and RMSE = 1.4 mm d<sup>-1</sup> when using modified parameterizations of  $Z_{om}$  and  $Rn_i$ .

According to our knowledge, there is little available information on the estimation of intra-orchard spatial variability of energy balance components and water requirements of super-intensive drip-irrigated olive orchards which represent heterogeneous woody canopies. Thus, the objective of this study is to evaluate the METRIC model for mapping the energy balance components, ETa and Kc for a super-intensive drip-irrigated olive orchard under Mediterranean climate conditions and to explore impacts of any heterogeneities.

## 1.1 Theory

The instantaneous net radiation calculate by METRIC for each pixel is calculated as follows (Allen et al., 2010);

$$Rn_i = (1 - \alpha) \cdot R_{s\downarrow} + R_{L\downarrow} - R_{L\uparrow} - (1 - \varepsilon_0) \cdot R_{L\downarrow} \quad (\text{Eq. 1.2})$$

where  $\alpha$  is the broadband surface albedo (dimensionless);  $R_{s\downarrow}$  is the incoming shortwave radiation ( $\text{W m}^{-2}$ );  $R_{L\downarrow}$  and  $R_{L\uparrow}$  are the incoming and outgoing longwave radiation, respectively and  $\varepsilon_0$  is the surface emissivity that accounts for reflectance of incoming longwave radiation at the land surface (Tasumi et al., 2005) . The computation of the broadband albedo is carried out by the integration of the surface reflectance for the visible and near infrared (NIR) bands using a weighting coefficient as (Tasumi et al., 2008) :

$$\alpha = \sum_{bd=1}^6 (\rho_{s,bd} \cdot w_{bd}) \quad (\text{Eq. 1.3})$$

where  $\rho_{s, bd}$  is at-surface (s) reflectance for each (bd) band (dimensionless) and  $w_{bd}$  is the weighting coefficient of the Landsat bands for calculating broad-band surface albedo (dimensionless) .

The instantaneous soil heat flux is computed using three empirical relations depending on the leaf area index (LAI). These functions were originally developed for annual crops as follows (Allen et al., 2010; Tasumi, 2003):

$$\frac{G_i}{Rn_i} = 0.05 + 0.18 \cdot e^{-0.52LAI} \quad (\text{if } LAI \geq 0.5) \quad (\text{Eq. 1.4})$$

$$\frac{G_i}{Rn_i} = 1.8 \cdot \frac{T_s}{Rn} + 0.84 \quad (\text{if } LAI < 0.5) \quad (\text{Eq. 1.5})$$

Also, a general equation was established to estimate  $G_i$  using the normalized difference vegetation index (NDVI) (W.G.M. Bastiaanssen et al., 1998):

$$\frac{G_i}{Rn_i} = T_s \cdot (0.0074 \cdot \alpha + 0.0038) \cdot (1 - 0.98 \cdot NDVI^4) \quad (\text{Eq. 1.6})$$

where  $T_s$  is the radiometric temperature ( $^{\circ}\text{C}$ ) computed from the thermal infrared waveband (TIR); LAI is expressed in ( $\text{m}^2 \text{m}^{-2}$ ); 0.0074 and 0.0038 are empirical coefficients and

Finally, METRIC estimates  $G$  for semi bare soil using the following equation (Allen et al., 2012):

$$\frac{G_i}{Rn_i} = 0.1 + 0.17e^{-0.55LAI} \quad (\text{Eq. 1.7})$$



The leaf area index is computed in METRIC using the next empirical relations(Allen et al., 2010):

$$\text{LAI} = 11 \cdot \text{SAVI}^3 \quad (\text{for } \text{SAVI} \leq 0.817) \quad (\text{Eq. 1.8})$$

$$\text{LAI} = 6 \quad (\text{for } \text{SAVI} > 0.817) \quad (\text{Eq. 1.9})$$

where SAVI is the soil adjusted vegetation index (dimensionless) calculated for each pixel (Basso et al., 2004).

Instantaneous pixel-by-pixel sensible heat fluxes are obtained for each scene as follows:

$$H_i = \frac{\rho_{\text{air}} \cdot C_p \cdot \Delta T_s}{r_{\text{ah}}} \quad (\text{Eq. 1.10})$$

where  $\rho_{\text{air}}$  is the air density ( $\text{kg m}^{-3}$ );  $C_p$  is the specific heat capacity of air ( $1,004 \text{ J kg}^{-1} \text{ K}^{-1}$ );  $\Delta T_s$  is the near-surface air temperature gradient ( $\Delta T_s = T_{a z1} - T_{a z2}$ ) above each pixel, where  $T_{a z1}$  and  $T_{a z2}$  are near surface air temperature ( $^{\circ}\text{K}$ ) at heights  $z_1$  and  $z_2$  above the elevation of  $d + z_{\text{om}}$ , where  $d$  is zero plane displacement height (m). The heights previously mentioned were in m.  $r_{\text{ah}}$  is the aerodynamic resistance to heat transport ( $\text{s m}^{-1}$ ). Originally, METRIC estimates the values of  $z_{\text{om}}$  based on the height ( $h$ ) of annual agricultural crops by assuming that the crop height vary proportionally with the LAI(Allen et al., 2010). Thus, for agricultural areas,  $z_{\text{om}}$  can be computed as follow:

$$z_{\text{om}} = 0.018 \cdot \text{LAI} \quad (\text{Eq. 1.11})$$

Bastiaanssen et al. (1998)and (Allen et al., 2007a) have demonstrated that  $\Delta T_s$  can be spatially approximated as a simple linear function:

$$\Delta T_s = \beta_0 + \beta_1 T_s \quad (\text{Eq. 1.12})$$

where  $\beta_0$  and  $\beta_1$  are empirical calibration coefficients for each satellite scene.  $T_s$  is expressed in K.

The iteration process based on the selection of several well-known anchor pixels (wet and dry) is to determine the unknown values of  $\beta_0$  and  $\beta_1$  for each scene due to the values of  $T_s$  for each pixel. The conditions for determining the anchor points are represented by an agricultural field with full and active transpiration vegetation close to reference conditions (cold pixel) and a surface with no vegetation cover (hot pixel) with little or residual evaporation from soil (Kjaersgaard et al., 2009). In this manner, the surface energy balance (SEB) of the cold pixel can be computed as:

$$H_{\text{cold}} = Rn_{\text{cold}} - G_{\text{cold}} - \phi \cdot \lambda ETr_h \quad (\text{Eq. 1.13})$$

where  $H_{\text{cold}}$ ,  $Rn_{\text{cold}}$  and  $G_{\text{cold}}$  represent the sensible heat, net radiation and soil heat fluxes for each cold pixel located inside the image at the time of satellite overpass ( $\text{W m}^{-2}$ );  $ETr_h$  is the hourly reference evapotranspiration ( $\text{mm h}^{-1}$ );  $\phi$  is an adjustment factor which incorporates the probability of wet soil surface beneath the vegetation canopy that may increase the total  $ETr_h$  (Allen et al., 2007a). The hot pixel is calculated using the Eq. 1.13, assuming that  $\phi \lambda ETr_h$  is near to zero if it has been a long period without rain or irrigation. Otherwise an estimate for  $\phi \lambda ETr_h$  must be made using some form of hourly or daily soil water balance (Allen et al., 2007a). In this regard, Tasumi (2003) and Folhes et al. (2009) indicated that the evapotranspiration from full cover alfalfa is between 20-40% greater than clipped grass.

After obtaining the values of  $\beta_0$  and  $\beta_1$  from the anchor pixels, these values are used in the estimation of H for each pixel by an iterative process that involves the Monin-Obukhov similarity theory (Allen et al., 2007a; Kalma et al., 2008; Seguin et al., 1994). The self-calibration of METRIC involves the inverse calibration of the surface energy balance (SEB) via the sensible heat flux computed by specifying the evapotranspiration at the two anchor pixels. This process removes systematic biases embedded in the estimations of  $R_{ni}$ ,  $G_i$  and other intermediate components of the METRIC algorithm, which are common to nearly all satellite-based calculations.

Finally, the instantaneous ( $ET_{a_i}$ ) and daily ( $ET_a$ ) values of actual evapotranspiration are calculated using the following equation:

$$ET_{a_i} = 3,600 \cdot \frac{LE_i}{\lambda \rho_w} \quad (\text{Eq. 1.14})$$

$$ET_a = ET_{rF} \cdot ET_{r24} \quad (\text{Eq. 1.15})$$

where  $ET_{a_i}$  and  $ET_a$  are in  $\text{mm h}^{-1}$  and  $\text{mm day}^{-1}$ , respectively; 3,600 converts from seconds to hours,  $\rho_w$  is the density of the water ( $\sim 1000 \text{ kg m}^{-3}$ );  $ET_{rF}$  is reference evapotranspiration fraction at the time of satellite overpass; and  $ET_{r24}$  is the reference evapotranspiration at 24 hours ( $\text{mm day}^{-1}$ ). Values of  $ET_{rF}$  are computed as:

$$ET_{rF} = Kc = \frac{ET_{a_i}}{ET_{r_h}} \quad (\text{Eq. 1.16})$$

where  $ET_{rF}$  is the same as the crop coefficient ( $Kc$ ) because it is assumed that  $ET_{rF}$  is equal to the mean value of hourly ratios of  $ET_{a_i}$  to  $ET_{r_h}$  for the daytime period (Allen et al., 2007b; D. Colaizzi et al., 2006; Gowda et al., 2008; Tasumi et al., 2005; Trezza,

2006). According to Allen et al. (2007),  $ET_{rh}$  is estimated over a standardized 0.5 m tall alfalfa.

Values of  $ET_{O_{24}}$  and  $ET_{oh}$  (clipped grass reference) using the Penman-Monteith model are calculated as follows (Allen et al., 2005, 1998):

$$ET_{O_{24}} = \sum_{i=1}^{24} ET_{oh} \quad (\text{Eq. 1.17})$$

$$ET_{oh} = \frac{0.408 \cdot \Delta \cdot (Rn_g - G_g) + \gamma \frac{C_n \cdot u \cdot VPD}{(Ta + 273.16)}}{\Delta + \gamma \cdot (1 + C_d \cdot u)} \quad (\text{Eq. 1.18})$$

where  $Rn_g$  is the net radiation over a short reference alfalfa or grass ( $\text{MJ m}^{-2} \text{h}^{-1}$ ),  $G_g$  is the soil heat flux for short reference ( $\text{MJ m}^{-2} \text{h}^{-1}$ );  $\gamma$  is the psychrometric constant ( $\text{kPa } ^\circ\text{C}^{-1}$ );  $Ta$  is air temperature for short reference surface ( $^\circ\text{C}$ );  $u$  is the mean wind speed at 2-m height ( $\text{m s}^{-1}$ );  $VPD$  is the vapor pressure deficit ( $\text{kPa}$ );  $\Delta$  is the slope of the saturation curve ( $\text{kPa } ^\circ\text{C}^{-1}$ );  $C_n$  is the denominator conversion factor (37 for the clipped grass reference); and  $C_d$  is the denominator conversion factor (0.24 and 0.96 for daytime and nighttime, respectively for the clipped grassreference).

## CHAPTER 2 MATERIALS AND METHODS

### 2.1 Study field

The study was conducted during two growing seasons (2011-2012 and 2012-2013) in a superintensive drip-irrigated olive (*Olea europaea* L. cv Arbequina) orchard established in 2005 and located in Penuhue Valley, Region del Maule, Chile (35° 23' LS; 71° 44' LW; 96 m above sea level) (Figure 2.1). The climate is Mediterranean with an annual rainfall of 620 mm concentrated in the winter period (Ahumada-Orellana et al., 2017). Cumulative  $E_{Tr24}$  and average daily temperature are 1160 mm and 14.8 °C for the growing seasons (from September to April), respectively. The soil texture is clay-loam (31% clay, 29% sand, and 40% silt), with a bulk density of 1.34 g cm<sup>-3</sup>, a field capacity of 0.31 cm<sup>3</sup> cm<sup>-3</sup>, and a wilting point of 0.16 cm<sup>3</sup> cm<sup>-3</sup> at the effective rooting depth (0–60 cm).

The olive trees for oil production were trained under a hedgerow system with a planting density of 1333 tree ha<sup>-1</sup> (1.5 x 5.0 m) and irrigated using two drippers (2.0 L h<sup>-1</sup>) per tree (Figure 2.2). The wetted area of the drip-irrigated orchard was only about 4.5% of the total area and was located below canopy. For the two growing seasons, the tree trunk diameters ranged between 61-73 mm while the tree height (h) and canopy width were 3.2 and 1.55 m, respectively.

### 2.2 Irrigation management and plant measurements

To evaluate the orchard irrigation management, the midday stem water potential ( $\psi_x$ ) was monitored using a pressure chamber (PMS instruments, model 600, Albany, OR, USA). This was done using a shoot (two per tree) with five or six pairs of leaves which was

encased in a plastic bag and wrapped in aluminium foil at least 2 h before the cut of the shoots (Tognetti et al., 2007) .

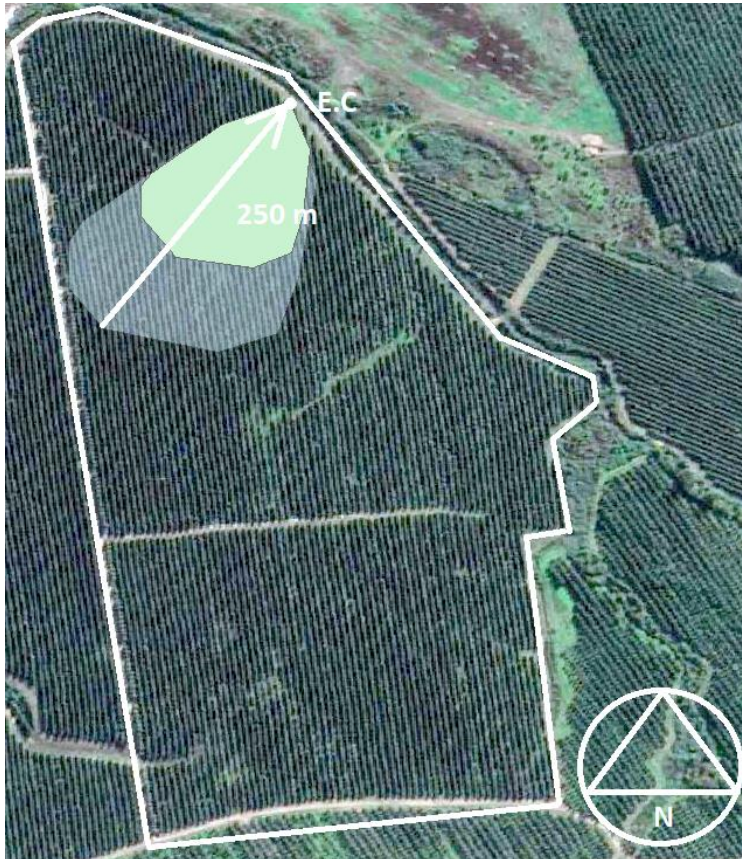


**Figure 2.1.** Experimental site with drip-irrigated olive trees (Quepo, Penciahue Valley, Maule Region, Chile). White dot shows the location of the eddy covariance (EC) system and the arrow represents the typical wind direction towards the EC system at the time of satellite overpasses. The transparent area represents the average footprint area and the light green area was used to sample pixels for validating the METRIC model to estimate energy balance components, evapotranspiration and crop coefficient on a pixel-by-pixel basis.

For this study, the fractional cover ( $f_c$ ) was estimated using the average canopy width and the number of trees per hectare (Er-Raki et al., 2008; López-Olivari et al., 2016). The average values of  $f_c$  ranged between 0.29-0.31 for the two growing seasons. For the

same olive orchard, Ortega-Farias et. al (2016) indicated that  $f_c$  was between 0.25–0.28 for the 2013/14 season when using a helicopter-based unmanned aerial vehicle (UAV) equipped with a multispectral camera.



**Figure 2.2** Experimental site of a drip-irrigated olive orchard (November 2013, Penuhue Valley, Maule Region of Chile).

### **2.3 Energy balance measurements**

A tower was installed in an experimental plot (21.1 ha) located within the olive orchard (1400 ha) in order to measure micrometeorological variables and orchard energy balance components at 30 min intervals. Air temperature ( $T_a$ ) and relative humidity (RH)

were measured using a vaisala probe (model HMP45C) while wind speed ( $u$ ) and wind direction ( $w$ ) were monitored by a cup anemometer and wind vane (03101-5, Young, MI, USA). The net radiation ( $R_n$ ) and solar radiation ( $R_s$ ) were measured using by a Fritchen type net radiometer (Q7.1, REBS Inc., Bellevue, WA, USA) and Silicon Pyranometer (LI200X, Campbell Scientific Inc., Logan, Utah, USA), respectively.

The sensible heat flux ( $H$ ) and latent heat flux ( $LE$ ) were measured using an eddy covariance (EC) system oriented towards the predominant wind direction (south-east). Values of  $H$  and  $LE$  were measured at 10 Hz using a three-dimensional sonic anemometer (CSAT3, Campbell Sci., Logan, UT, USA) and a fast response open-path infrared gas analyzer (LI-7500 IRGA; LI-COR, Inc., Lincoln, NE, USA) respectively. Means, standard deviations and covariances were calculated over 30-min periods. In the tower, sensors of EC fluxes ( $H$  and  $LE$ ) and meteorological variables ( $T_a$ ,  $RH$ ,  $u$ ,  $w$ ,  $R_s$  and  $R_n$ ) were installed at 2.3 and 1.8 m above the center of the tree canopy (Figure 2.4).

Upwind fetch of the prevailing wind direction was 250 m (interrupted only by internal olive orchard roads) (Figure 2.3). The source area (footprint) for the turbulent fluxes, which corresponds to the contributing surface patches to scalar flux measurements from the EC system was calculated using the model proposed by Kljun et al., 2015 who have an available code for several programming languages at [www.footprint.kljun.net](http://www.footprint.kljun.net). Finally, the footprint analysis indicates that the source area was similar for the clear days used in this study (Figure 2.3). The footprint size did not significantly change and did not substantially affect the area used for validation. The upwind fetch of the prevailing wind direction ranged between 200-250 m which provided sufficient fetch for the footprint areas to be used for validation.



Soil heat flux ( $G$ ) was estimated using a weighting of eight flux plates (HP) placed in the inter-row (positions 1, 2, 7 and 8) and below the tree canopy (positions 2, 3, 5 and 6) (Figure 2.5). The weighting was based on fraction of ground cover at solar noon (see Eq. 2.3). These plates of constant thermal conductivity (HFT3, Campbell Sci., Logan, UT, USA) were placed at a 0.08 m depth. Two averaging thermocouple probes (TCAV, Campbell Sci., Logan, UT, USA) for measuring soil temperature ( $T_{\text{soil}}$ ) were installed above each flux plate at depths of 0.02 and 0.06 m. Thermocouple probe signals were recorded at 30-min intervals on an electronic datalogger (CR3000, Campbell Sci, Logan, UT, USA).

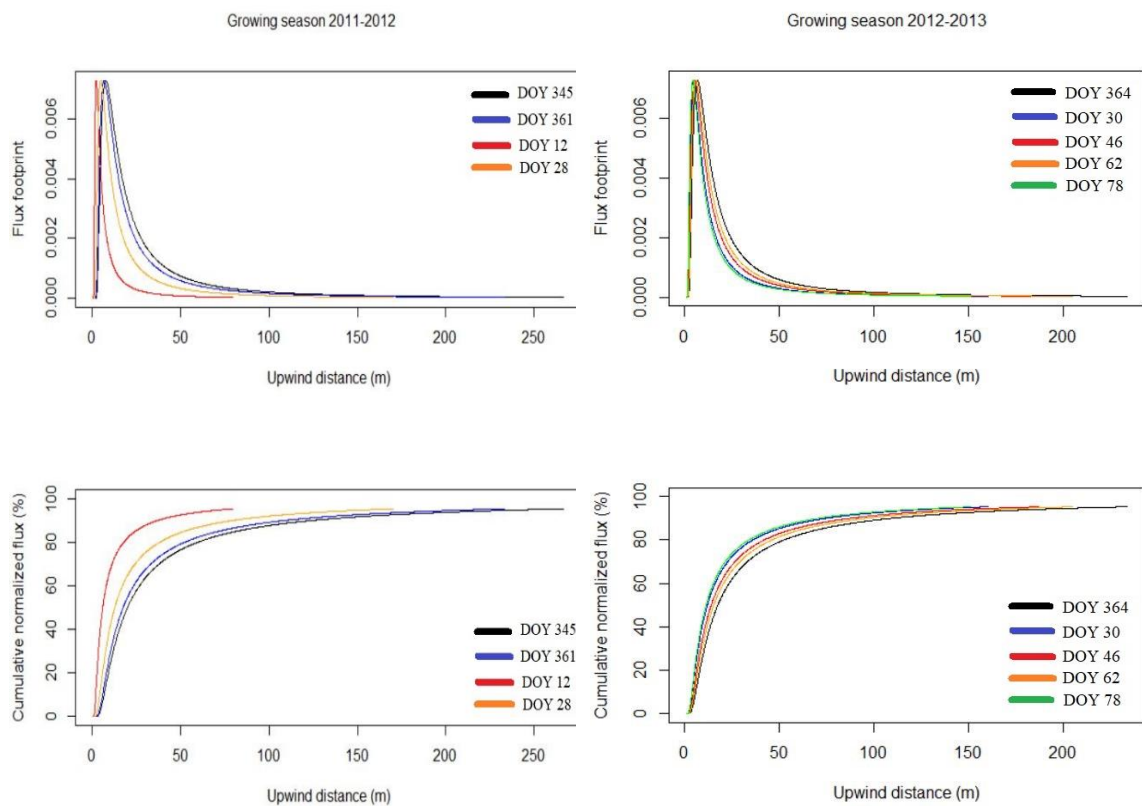


**Figure 2.3.** Analytical footprint model under unstable conditions in terms of relative and cumulative contribution, respectively for the days used in this study.

At each position,  $G$  was estimated using the following equations (Oliphant et al., 2004; Ortega-Farías et al., 2016; Shao et al., 2008):

$$G = FP + S \quad (\text{Eq. 2.1})$$

$$S = \left( \rho_b C_d + \theta_g \rho_w C_w \right) \frac{\Delta T_{\text{soil}}}{\Delta t} d \quad (\text{Eq. 2.2})$$

where  $FP$  are fluxes measured flux at 0.08 m,  $S$  is the heat stored in the layer above the heat flux plates,  $\rho_b$  is the soil bulk density ( $1600 \text{ kg m}^{-3}$ );  $\rho_w$  is the density of water ( $1000 \text{ kg m}^{-3}$ );  $C_d$  is the specific heat capacity of soil ( $890 \text{ J kg}^{-1} \text{ K}^{-1}$ );  $C_w$  is the specific heat capacity of the soil water ( $4190 \text{ J kg}^{-1} \text{ K}^{-1}$ );  $\Delta T_{\text{soil}}$  is the change in soil temperature (K);  $\Delta t$  is the time intervals (s).

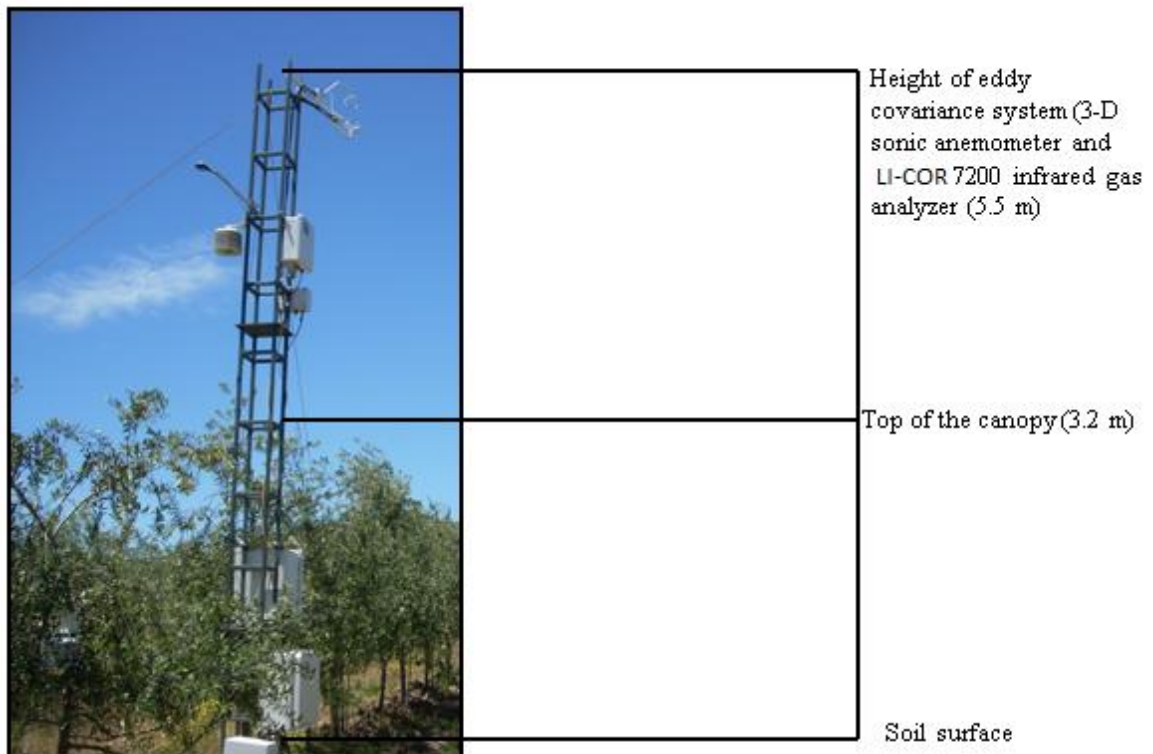


**Figure 2.4.** Eddy Covariance system installed within the experimental site (November 2013, Pencahue Valley, Maule Region of Chile)

Finally, the average values of  $G$  for the orchard were weighted by fractional cover ( $f_c$ ):

$$G = G_{UO}f_c + (1 - f_c)G_{BR} \quad (\text{Eq. 2.3})$$

where  $G_{UO}$  and  $G_{BR}$  are the average  $G$  value ( $\text{W m}^{-2}$ ) below the canopy and between rows, respectively (Figure 2.5).

At 2 km from the experimental plot, an automatic weather station was installed above a reference grass to measure meteorological variables that were used as input in the FAO56 Penman-Monteith equation to compute the reference evapotranspiration ( $ET_o$ ) at 30-min intervals.

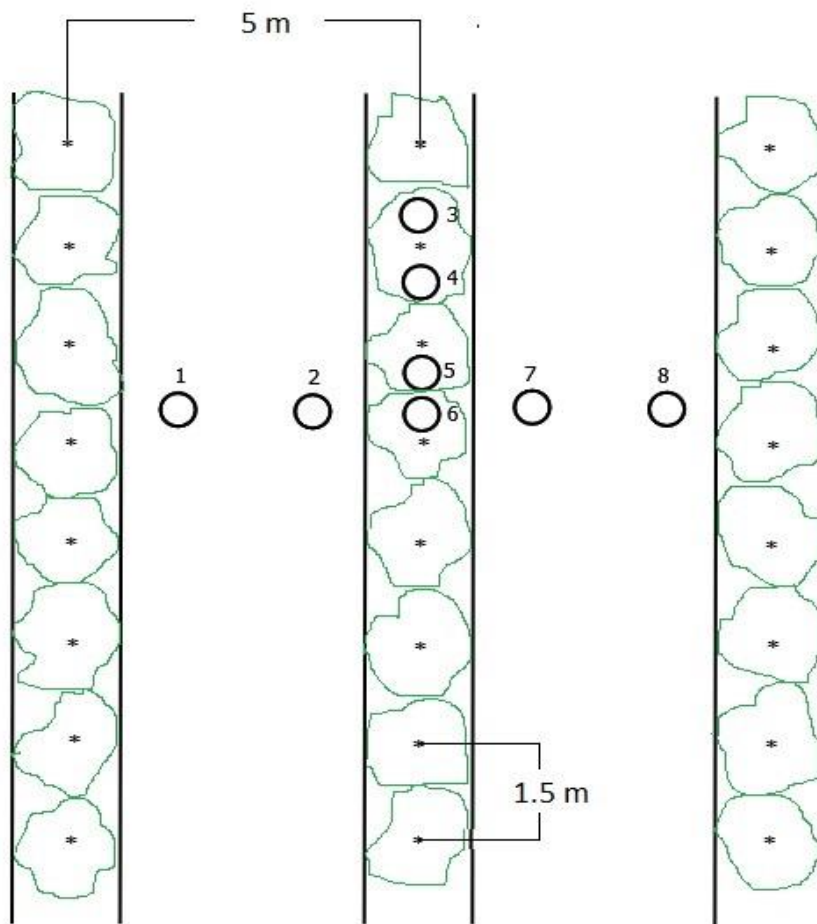


**Figure 2.5.** Distribution of soil heat flux ( $G$ ) measurements for a drip-irrigated olive orchard. The positions 1,2,7 and 8 indicated that fluxes were measured between rows while positions 3, 4, 5 and 6 show that fluxes were obtained below the tree canopy (3, 4, 5 and 6). Also, the asterisks and open circles indicate the location of drippers and  $G$  measurements, respectively.

## 2.4 Data quality control

For model validation, it is necessary to avoid systematic errors in the EC measurements of turbulent fluxes. In this matter, Twine et al., (2000) indicated that a systematic error that underestimates the evapotranspiration component of a crop water budget by 25% is intolerable to an irrigation scheduler. For this reason, days presenting energy balance closure (EBc)  $((H+LE)/(Rn-G)) < 0.7$  or  $> 1.2$  were excluded from this study to reduce the uncertainty associated with errors in the LE measurements (de la Fuente-Sáiz et al., 2017; López-Olivari et al., 2016; Ortega-Farias et al., 2010). These errors can be related to persistent noisy behavior due to sensor problems, flow distortion through the tower, or adverse meteorological conditions (for example rainy days). Also, Twine et al (2000) suggested that the Bowen Ratio (ratio of H to LE) is measured accurately by the EC system because the different problems affect in a similar proportion to the measured values of H and LE. Thus, LE values from the EC system were recalculated as follows (Er-Raki et al., 2008; Martínez-Cob and Faci, 2010; Twine et al., 2000):

$$LE_{BR} = \frac{Rn-G}{1+\beta} \quad (\text{Eq. 2.4})$$

where  $LE_{BR}$  = latent heat flux corrected using the Bowen Ratio ( $W m^{-2}$ );  $\beta$  = Bowen Ratio (dimensionless). 30-min values of  $LE_{BR}$  were converted to daily olive evapotranspiration using the following expression:

$$ET_{BR} = \frac{\sum_{i=1}^{48} LE_{BR}}{\lambda\rho_w} Cf \quad (\text{Eq. 2.5})$$

where  $ET_{BR}$  = olive evapotranspiration by the EC system ( $\text{mm d}^{-1}$ );  $C_f$  = conversion factor (1800);  $\rho_w$  = density of water ( $1,000 \text{ kg m}^{-3}$ );  $\lambda$  = latent heat of vaporization ( $\text{J kg}^{-1}$ );  $i$  = number of measurements over a 24 hour period (48 measurements from 00:00 to 23:30 hours).

## 2.5 Satellite images

For the two growing seasons, 19 Landsat 7 (+ETM) satellite scenes (Path 233, Row 85) were available from the USGS Glovis (“USGS Global Visualization Viewer,” n.d.). However, nine satellite images were used in this research because 6 and 4 images presented a cloud cover  $> 30\%$  and  $EBC < 0.70$ , respectively (Table 2.1). All Landsat scenes acquired and used in this work include a default for the systematic radiometric and geometric corrections which consider ground control points and a Digital Elevation Model (DEM) for topographic accuracy standard terrain correction (Level 1T-precision and terrain correction).

**Table 2.1.** Images selected for processing surface energy balances over a drip-irrigated olive orchard with their percentage cloud covering.

Growing Season	Date (mm-dd-yy)	DOY	Overpasses time (local time)	Cloud Cover (%)
2011-2012	12/11/2011	345	11:28 am	2.0
	12/27/2011	361	11:28 am	2.0
	01/12/2012	12	11:28 am	0.0
	01/28/2012	28	11:28 am	1.0
2012-2013	12/29/2012	364	11:30 am	2.0
	01/30/2013	30	11:30 am	1.0
	02/15/2013	46	11:30 am	1.0
	03/03/2013	62	11:30 am	1.0
	03/19/2013	78	11:30 am	3.0

The energy balance components were calculated on a pixel-by-pixel basis and averaged over 15 pixels departing from the tower station in the main wind direction (Figure 2.1).

This area was delimited by the Flux Footprint Prediction (FFP) of the turbulent fluxes using the model proposed by Kljun et al. (2015). The coefficient of variation (CV) of NDVI was considered to see if the footprint is constant.

## 2.6 Images processing

### 2.6.1 Functions from literature

In this study, calibrated sub-models from the literature for olive orchards were included in the original METRIC model to simulate values of LAI,  $z_{om}$  and  $G$ . In this case, values of LAI were estimated according to Santos et al. (2012):

$$LAI = \frac{\ln \left[ \frac{0.69 - SAVI}{0.59} \right]}{0.91} \quad (\text{Eq. 2.6})$$

where LAI is the leaf area index modeled by a satellite scene at each pixel ( $\text{m}^2 \cdot \text{m}^{-2}$ ).

The Perrier function for estimating  $z_{om}$  has been suggested to compute  $z_{om}$  in sparse canopies such as olive orchard. In this study, values of  $z_{om}$  were estimated using the following equation (Pôças et al., 2014; Santos et al., 2012):

$$z_{om} = \left( \left( 1 - e^{-\alpha \frac{LAI}{2}} \right) \cdot e^{-\alpha \frac{LAI}{2}} \right) \cdot h \quad (\text{Eq. 2.7})$$

where  $\alpha$  is the coefficient ( $\alpha = 0.83$ ) and  $h$  is the height of canopy ( $h = 3.2$  m) (Santos et al., 2012). In this regard, Santos et al. (2012) indicated that the Perrier function in the METRIC model reduced the RMSE from 1.12 to 0.25  $\text{mm day}^{-1}$ .

In comparison from the original METRIC equation (Eq. 1.11), shows that the Perrier equation gives better performance in the calculation on ETa for sparse orchard like olives.

Finally, values of G were estimated according to the following linear equation (Ortega-Farías et al., 2016):

$$G=0.324 \cdot R_n - 51.5 \quad (\text{Eq. 2.8})$$

Equation 2.8 was developed using a database collected for an olive orchard during the 2009/10 and 2010/11 growing seasons. Ortega-Farias et al (2016) indicated that equation 2.8 was able to predict G with an error of 2% when using Thermal and Multispectral Cameras Placed on a Helicopter-Based Unmanned Aerial Vehicle (UAV). Also, Fuentes-Peñailillo et al., (2018) observed that equation 2.8 predicted G with an error of 8% when using satellite images (Landsat 7 ETM+). In addition, the following calibrated sub-models of G for vineyard (Eq. 2.9, Carrasco-Benavides et al., 2014) and apple orchard (Eq. 2.10, de la Fuente-Sáiz et al., 2017) were evaluated:

$$\frac{G_i}{R_{n_i}} = T_s (0.0059\alpha + 0.0034)(1 - 0.98NDVI^4) \quad (\text{Eq. 2.9})$$

$$\frac{G_i}{R_{n_i}} = T_s (0.00261\alpha + 0.001)(1 - 0.98NDVI^4) \quad (\text{Eq. 2.10})$$

### 2.6.2 MATLAB code

A MATLAB script was implemented to simulate SEB, ETa and Kc using the METRIC algorithm with the objective of reducing the time image processing. Figure 2.6 shows different steps for the image processing. After the satellite images are downloaded manually from USGS Glovis, the scripts starts on making a stacking layer of the bands blue, green, red, near-infrared (NIR), and short-wave infrared (SWIR). Then each images are cropped in the influenced area to select the cold and hot pixels and the gaps were filled (Chen et al., 2011) for each cropped image, and eliminate the cloud using

NASA method. Finally, the script runs the original METRIC until the hot and cold pixels are selected using the methodology of Kjaersgaard et al. (2009). Once the values of  $\beta_0$  and  $\beta_1$  are obtained and  $\Delta T_s$  is calculated (Eq. 1.11), the equations 2.6, 2.7 and 2.8 are used to estimate  $ET_a$  for the studied area. Finally, the adjustment factor ( $\phi$ ) was assumed 1.2 for estimating  $H_{cold}$ .

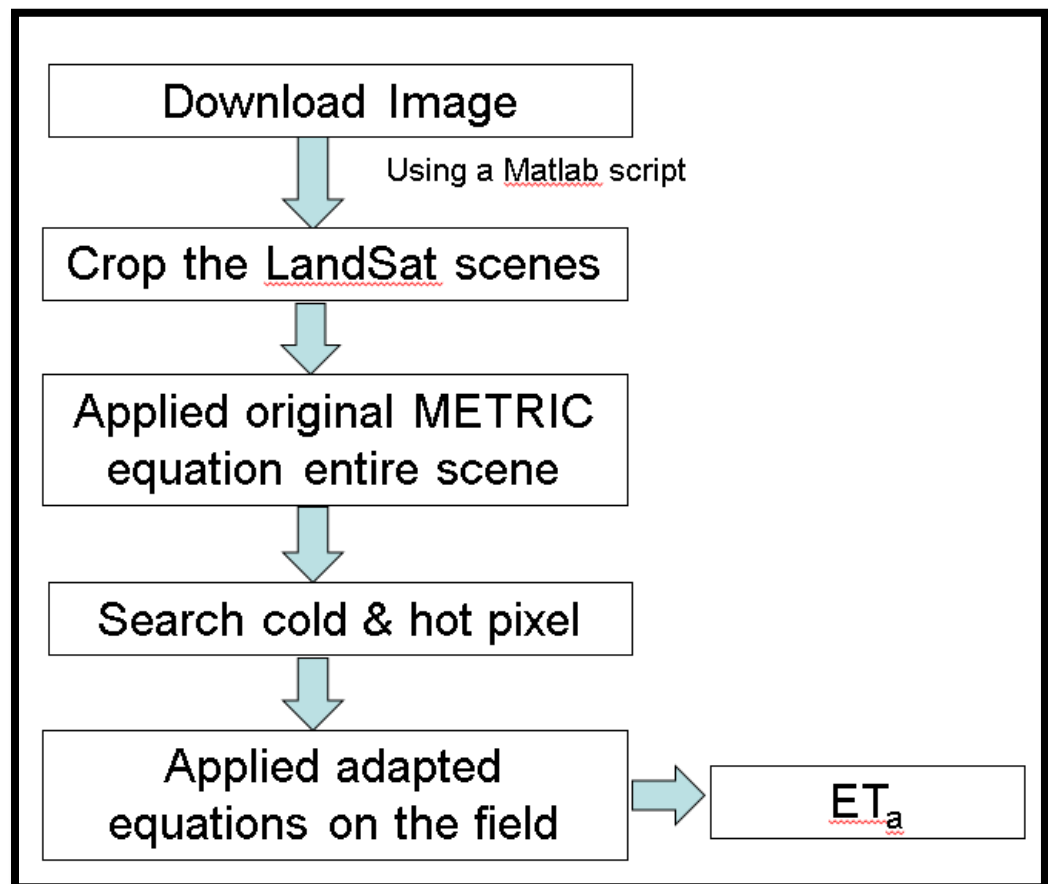


**Figure 2.6.** Flowchart of MATLAB code for image processing.

## 2.7 Statistical validation

Instantaneous satellite-based estimates of  $R_n$ ,  $G$ ,  $H$ ,  $LE$ ,  $ET_a$  and  $K_c$  were computed by averaging values of 15 (30 m x 30 m) pixels. To avoid the “contamination”



caused by pixels outside the experimental plot, a perimeter of 30 m from the edges inward was excluded when calculating field-scale average SEB fluxes. The validation was carried out using the ratio (b) of estimated to observed values, root-mean-square error (RMSE), mean absolute error (MAE), index of agreement (Ia) and root-mean-square error (RMSE). Values of RMSE, MAE and Ia were computed using the following equations:

$$\text{RMSE} = \sqrt{\frac{\sum_{i=1}^N (P_i - O_i)^2}{N}} \quad (\text{Eq. 2.11})$$

$$\text{MAE} = \frac{\sum_{i=1}^N |P_i - O_i|}{N} \quad (\text{Eq. 2.12})$$

$$I_a = 1 - \left[ \frac{\sum_{i=1}^N (P_i - O_i)^2}{\sum_{i=1}^N (|P_i - \bar{O}| + |O_i - \bar{O}|)^2} \right] \quad 0 \leq I_a \leq 1 \quad (\text{Eq. 2.13})$$

where N is the total number of observations,  $P_i$  and  $O_i$  are the estimated and observed values, respectively, and  $\bar{O}$  is the mean of the observed values. Values of RMSE, MAE,  $P_i$ ,  $O_i$ , and  $\bar{O}$  are in  $\text{W m}^{-2}$  or  $\text{mm d}^{-1}$ .

Finally, the student's *t*-test was used applied to evaluate whether b was significantly different from unity at the 95% confidence level.

## CHAPTER 3. RESULTS AND DISCUSSION

### 3.1 Climatic conditions and energy balance ratios

Generally, the atmospheric conditions at the drip-irrigated olive orchard were hot and dry with  $ET_{r24}$  ranging between 4.7-8.9 mm day<sup>-1</sup> (Table 3.1). At the time of satellite overpass, values of air temperature ( $T_a$ ), vapor pressure deficit (VPD) and wind speed ( $u$ ) were between 15.7-23.1 °C, 0.79-1.85 kPa and 0.52-2.34 m s<sup>-1</sup>, respectively.

Predominant wind directions were between 140-235° which presented a frequency distribution of 89.3 and 93.4% of total observations for the first and second seasons. Finally, values of the midday stem water potential ( $\psi_x$ ) ranged from -1.3 to -1.80 MPa indicating that the olive trees were under well-irrigated conditions during the two seasons (Ahumada-Orellana et al., 2017; Gómez-del-Campo et al. 2008; Moriana et al. 2007). In this case, the total irrigation application was 1830 and 2014 m<sup>3</sup> ha<sup>-1</sup> for the first and second seasons respectively.

The accuracy of the EC measurements above the olive orchard was evaluated using the energy balance closure which presented a coefficient of determination of 0.9 for the two study periods (Figure 3.1). At 30-minute time interval, Also, EBC was equal to 0.85 indicating that the orchard energy balance was systematically imbalanced by about 15 %. At the time of satellite overpass, the mean value of EBC ranged between 0.75 and 1.11 (Table 3.2). Literature has indicated that turbulent fluxes (H+LE) were less than available energy for olive orchard with EC imbalances ranging between 5% and 26% (Er-Raki et al., 2010, 2008; Ezzahar et al., 2007; Martínez-Cob and Faci, 2010; Ortega-Farías and López-Olivari, 2012; Testi et al., 2006; Villalobos et al., 2000).

These imbalances may be associated to errors in the measurements of Rn and G (Lee and Black, 1993; Leuning et al., 2012; Wilson et al., 2002), energy storage within the olive tree biomass (Williams et al., 2004), low wind speed (Testi et al., 2004) and heterogeneity of surface energy balance of the region (Foken, 2008). According to several researchers, the EC imbalances observed in this study are considered appropriate to provide accurate estimates of turbulent fluxes (HE + LE), especially following the Bowen-ratio approach adjustment (Eq. 2.4 and 2.5) ( Er-Raki et al. 2008; Martínez-Cob and Faci, 2010; Twine et al., 2000).

**Table 3.1.** Mean daily values of air temperature (Ta), vapor pressure deficit (VPD), wind speed (u) and wind direction (w) at the time of satellite overpass. Also, daily reference evapotranspiration (ETr) is included.

Season	DOY	Ta (°C)	VPD (kPa)	U (m s <sup>-1</sup> )	w (degrees)	ETr (mm day <sup>-1</sup> )
2011-2012	345	19.6	1.47	2.34	200	8.9
	361	23.1	1.71	1.17	236	8.7
	12	21.7	1.85	0.84	179	7.9
	28	19.4	1.35	1.39	161	7.4
2012-2013	364	19.7	1.23	1.15	180	7.7
	30	20.8	1.30	0.83	226	7.1
	46	21.9	1.35	0.41	202	7.3
	62	19.0	1.22	0.38	140	6.3
	78	15.7	0.79	0.52	161	4.7

Table 3.2 indicates that ratios of Hi to Rni were between 0.50-0.61 while those of LEi to Rni ranged between 0.14-0.25 for the two growing season. Also, values of Gi/Rni ratios were between 0.17-0.36 and Bowen ratios ( $\beta$ ) fluctuated between 2.3-4.0. This analysis indicated that the main component of the Rni partitioning was the sensible heat flux (Hi) over the drip-irrigated olive orchard which presented a fractional cover of 0.3. For a super-intensive drip-irrigated olive orchard ( $f_c = 0.3$ ), López-Olivari et al. (2016) indicated that daily values of LE, H and G were between 0.28–0.47, 0.34–0.68 and 0.02–

0.06 of  $R_n$ , respectively, while annual mean Bowen ratios ( $\beta$ ) varied between 1.22 and 1.64. For olive orchards ( $f_c$  ranging between 0.13-0.47), Ramírez-Cuesta et al. (2019) observed that mean ratios of instantaneous LE, H and G to  $R_n$  at the time of satellite overpass were 0.51, 0.33 and 0.16, respectively when using Landsat satellite images (pixels = 30 m x 30m). Also, these authors observed that  $\beta$  varied between 0.64-0.83 indicating that the main component of the  $R_n$  partitioning was LE. Finally, Testi et al. (2005) indicated that values of  $\beta$  depend on the leaf area index (LAI) and soil water content.

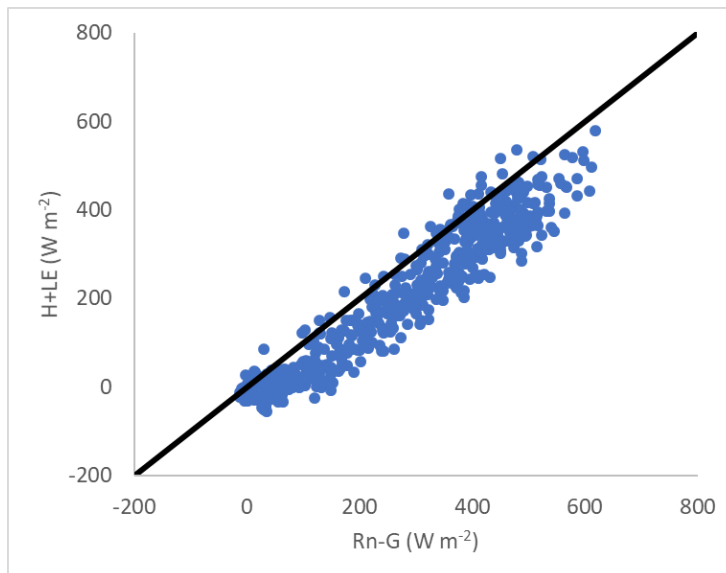


**Figure 3.1.** Energy balance closure (EBC) at 30-min intervals for days when satellite overpassed during 2011-2012 and 2012-2013 growing season. Days presenting values of EBC  $< 0.7$  or  $> 1.3$  were excluded from this study to reduce the uncertainty associated with errors in the LE measurements

**Table 3.2.** Energy balance closure (EB<sub>c</sub>), Bowen ratio ( $\beta$ ) and instantaneous ratios of latent (LE $\beta$ i), sensible (H $\beta$ i) and soil (Gi) heat fluxes to net radiation (R<sub>ni</sub>) for a drip-irrigated orchard. Instantaneous ratio of R<sub>n</sub> to incoming solar radiation (R<sub>s</sub>) is also included.

Season	DOY	EB <sub>c</sub>	R <sub>ni</sub> /R <sub>si</sub>	$\beta$	H $\beta$ i/R <sub>ni</sub>	LE $\beta$ i/R <sub>ni</sub>	Gi/R <sub>ni</sub>
2011-2012	345	0.75	0.68	4.03	0.58	0.14	0.28
	361	0.86	0.69	3.17	0.57	0.18	0.26
	12	0.79	0.67	3.52	0.55	0.15	0.3
	28	0.79	0.67	3.6	0.5	0.14	0.36
2012-2013	364	0.81	0.72	2.38	0.59	0.25	0.17
	30	0.75	0.69	2.56	0.57	0.22	0.21
	46	0.80	0.69	2.29	0.58	0.25	0.16
	62	0.78	0.68	2.4	0.56	0.23	0.21
	78	1.11	0.65	3.4	0.61	0.18	0.21
<b>Mean</b>		<b>0.83</b>	<b>0.68</b>	<b>3.04</b>	<b>0.57</b>	<b>0.19</b>	<b>0.24</b>

Note: The data from this table correspond to ground-truth measurements at the satellite overpass.

### 3.2 Comparison between Measured and Estimated Variables

#### 3.2.1 Evaluation of sub model to estimate soil heat flux

Table 3.3 indicates that the Eq. 1.7 (Allen et al., 2012) and 2.8 (Ortega-Farías et al., 2016) computed Gi with errors of 7 and 5 %, respectively. In addition, values of RMSE and MAE for Eq. 1.7 were 35 and 30 W m<sup>-2</sup> while those for Eq. 2.8 were 30 and 33 W m<sup>-2</sup>, respectively. These results are adequate considering that they are within the ranges observed in the literature (Carrasco-Benavides et al 2012; Ortega-Farías et al., 2016). Using a remote sensing model, Shaomin et al., (2007) suggested that errors in the estimation of G over complex canopies could be attributed to differences in spatial/temporal scales between satellite data and ground-truth measurements. According to these results, Eq. 2.8 was used in this study to simulate ET<sub>a</sub> and K<sub>c</sub> using the METRIC model.

**Table 3.3.** Evaluation of calibrated sub-models to estimate soil heat flux ( $G_i$ ) a super-intensive drip-irrigated olive orchard at the time of satellite overpass.

Sub-models	RMSE ( $W \cdot m^{-2}$ )	MAE ( $W \cdot m^{-2}$ )	b	Ia	t-test	Mean ( $W \cdot m^{-2}$ )
Eq. 1.6	45	40	1.32	0.6	F	153
Eq. 1.7	35	30	1.07	0.5	F	123
Eq. 2.8	40	33	1.05	0.49	F	122
Eq. 2.9	33	26	1.13	0.6	F	132
Eq. 2.10	116	106	0.55	0.3	T	230

RMSE = root mean square error; MAE = mean absolute error; b = ratio of observed to computed values; Ia = index of agreement; T = null hypothesis (b = 1) True; F = alternative hypothesis (b  $\neq$  1).

### 3.2.2 Comparison between the different fluxes

The comparisons between observed and estimated values of  $R_{si}$ ,  $R_{ni}$ ,  $H_i$ ,  $G_i$ , and  $LE_i$  at the time of satellite overpasses (11:28–11:30 h local time) are depicted in figure 3.2 for the olive orchard under well-irrigated conditions. This figure indicates that there was an equilibrated distribution of points around the 1:1 line for  $R_{si}$  and  $R_{ni}$  with RMSE and MAE ranging between of 29-43  $W \cdot m^{-2}$  (Table 3.4). The t-test indicated that the value of b was not significantly different from unity suggesting that the simulated and measured values of  $R_{si}$  and  $R_n$  were similar at the 95% confidence level. For a drip-irrigated olive orchard (fc between 26–30%), Fuentes-Peñailillo et al. (2018) observed that values of  $R_{ni}$  and  $G_i$  were underestimated with errors of 4 and 8%, respectively, when using Landsat satellite images (pixels = 30 m x 30m). In the same olive orchard, Ortega-Farías et al. (2016) indicated that  $R_{ni}$  and  $G_i$  were computed with less than 5% errors when using high-resolution thermal and multispectral data acquired with an UAV.

**Table 3.4.** Validation of sub-models to estimate incoming solar radiation (Rsi), net radiation (Rn), sensible heat flux (H), soil heat flux (G), and latent heat flux (LE) of a super-intensive drip-irrigated olive orchard at the time of satellite overpass.

Variable	RMSE ( $\text{W}\cdot\text{m}^{-2}$ )	MAE ( $\text{W}\cdot\text{m}^{-2}$ )	b	Ia	t-test	Mean ( $\text{W}\cdot\text{m}^{-2}$ )
Rsi	43	35	1.00	0.93	T	819
Rni	29	26	0.98	0.93	T	537
Hi	46	41	0.97	0.72	F	288
Gi	40	33	1.05	0.4	F	122
LEi	45	32	0.95	0.62	F	127

RMSE = root mean square error; MAE = mean absolute error; b = ratio of observed to computed values; Ia = index of agreement; T = null hypothesis (b = 1) True; F = alternative hypothesis (b  $\neq$  1); MEAN = average values for measured fluxes.

Comparisons between measured and estimated values of Hi and LEi at the time of satellite overpasses show that the points were close to the 1:1 line (Figure 3.2). In this case, the METRC model underestimated the instantaneous sensible and latent heat fluxes with errors of less than 5% (Table 3.4). Values of RMSE and MAE for Hi were 46 and 41  $\text{Wm}^{-2}$  while those of LEi were 45 and 32  $\text{Wm}^{-2}$ , respectively. The best agreement between measured and estimated sensible heat fluxes was observed on DOY 30 (2013) where the differences between estimated (E) and observed (O) values were less than 15  $\text{W m}^{-2}$ . The greatest disagreement was observed on DOY 78 (2013) with a difference of 65  $\text{W m}^{-2}$  which was associated with the selection of hot and cold pixels. Also, the results of this study indicate that the estimation of LEi mainly depended on the computation of H which was the main component of Rni partitioning. Both, Carrasco-Benavides et al. (2014) in a vineyard, and de la Fuente et al. (2018) in an apple orchard, found that METRIC estimated instantaneous values of Hi and LEi with errors ranging between 5-16% when using the calibrated functions of LAI,  $z_{om}$  and Gi.

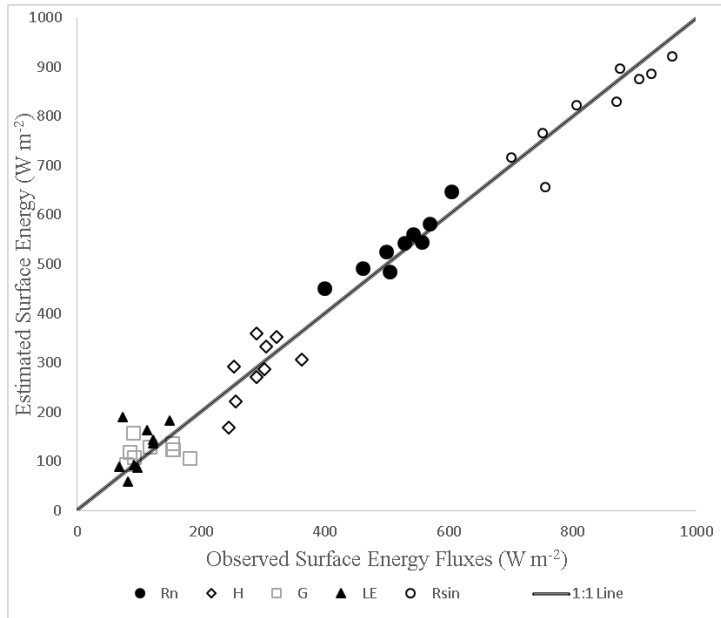


**Figure 3.2.** Comparisons at the time of satellite overpass between observed (axis X) and estimated (axis Y) values for net radiation (Rn), soil heat flux (G), sensible heat flux (H), latent heat flux (LE), and shortwave incoming radiation (Rsi) over a super-intensive drip-irrigated olive orchard for nine satellite-overpass days. The solid line represents the 1:1 line.

Furthermore, the model validation indicated that the METRIC model was able to simulate the ETa with RMSE = 0.42 mm day<sup>-1</sup> and MAE = 0.31 mm day<sup>-1</sup> (Table 3.5).

Additionally, the statistical analysis indicated that the b value was significantly different from unity suggesting that the METRIC model overestimated ETa with an error of 6.0 % of observed values. In this matter, Figure 3.3 indicates that most points were evenly distributed around the 1:1 line for a range of ETa between 1.1-3.5 mm day<sup>-1</sup>. Values of ETa from METRIC ranged between 1.1- 3.5 mm day<sup>-1</sup>, while those from the EC system were between 1.5- 3.5 mm day<sup>-1</sup> (Table 3.7). Finally, model validation indicates that values of Kc were simulated with an error of 4% and values of RMSE and MAE ranged between 0.05 and 0.09 (Table 3.5). For the super-intensive drip-irrigated olive orchard,



values of  $K_c$  fluctuated between 0.14-0.53 for METRIC model and 0.19-0.45 for the EC system (Table 3.7).

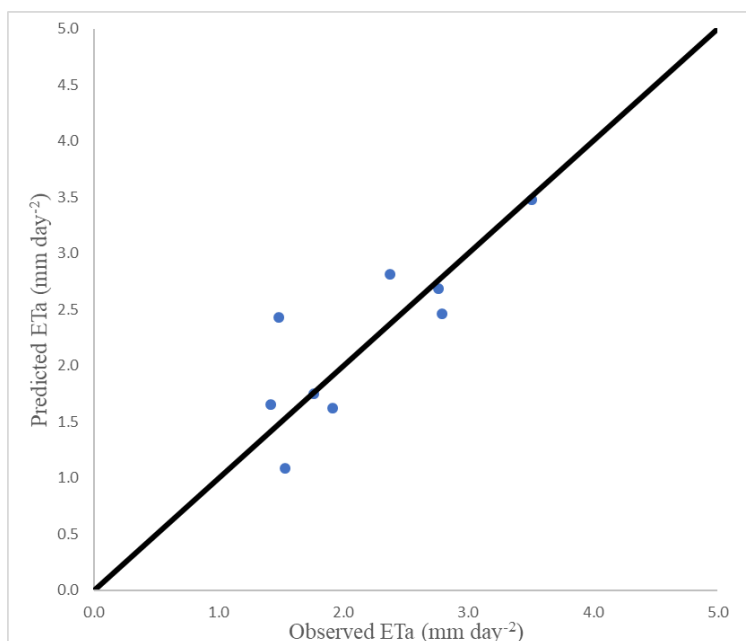


**Figure 3.3.** Daily comparisons between observed (axis X) and estimated (axis Y) values of actual evapotranspiration (ETa) of a super-intensive drip-irrigated olive orchard. The solid line represents the 1:1 line.

**Table 3.5.** Validation of METRIC model to estimate actual evapotranspiration (ETa) and crop coefficients ( $K_c$ ) of a super-intensive drip-irrigated olive orchard.

Variable	RMSE	MAE	b	Ia	t-test	MEAN
ETa (mm day <sup>-1</sup> )	0.42	0.31	1.06	0.87	F	2.2
$K_c$	0.09	0.05	0.96	0.96	F	0.27

RMSE = root mean square error; MAE = mean absolute error; b = ratio of observed to computed values; Ia = index of agreement; T = null hypothesis (b = 1) True; F = alternative hypothesis (b ≠ 1).

**Table 3.6.** Estimated and measured values of incoming solar radiation (Rsi), net radiation (Rni), soil heat flux (Gi), sensible heat flux (Hi) and latent heat flux (LEi) at the time of satellite overpass

Season	DOY	Rsi (W m <sup>-2</sup> )		Rni (W m <sup>-2</sup> )		Gi (W m <sup>-2</sup> )		Hi (W m <sup>-2</sup> )		LEi (W m <sup>-2</sup> )	
		Observed	Estimated	Observed	Estimated	Observed	Estimated	Observed	Estimated	Observed	Estimated
2011-2012	345	961	922	570	582	154	137	323	353	93	92
	361	927	887	557	544	154	125	306	333	97	87
	12	908	875	529	543	155	124	291	360	83	59
	28	872	830	504	485	183	106	253	292	69	88
2012-2013	364	877	896	604	647	90	158	363	306	150	183
	30	807	822	542	561	117	130	302	287	123	144
	46	752	765	499	526	86	119	290	272	123	136
	62	701	716	462	491	92	108	256	221	114	162
	78	756	656	399	451	80	95	245	168	74	189

**Table 3.7** Estimates and measured values of actual evapotranspiration (ETa) and grass-reference-based crop coefficient (Kc) at the day of satellite overpass

Season	DOY	ETa (mm day <sup>-1</sup> )		Kc	
		Observed	Estimated	Observed	Estimated
2011-2012	345	1.8	1.8	0.20	0.20
	361	1.9	1.6	0.20	0.20
	12	1.5	1.1	0.19	0.14
	28	1.4	1.7	0.19	0.23
2012-2013	364	3.5	3.5	0.45	0.44
	30	2.8	2.5	0.39	0.36
	46	2.8	2.7	0.38	0.39
	62	2.3	2.8	0.38	0.49
	78	1.5	2.4	0.32	0.53

**Table 3.8.** Coefficients of variation for sub-models over the footprint area to compute net radiation (Rn), sensible heat flux (H), soil heat flux (G), and latent heat flux (LE) of a super-intensive drip-irrigated olive orchard. Also, the normalized difference vegetation index (NDVI) is included. The degrees of freedom (n)= 23123 pixels.

Season	DOY	Rni (%)	LE (%)	Hi (%)	Gi (%)	NDVI (%)
2012-2013	364	0.60	8.59	3.12	1.41	3.80
	30	0.80	13.17	4.25	1.39	4.21
	46	0.80	9.96	3.97	1.32	4.28
	62	0.84	9.29	5.12	1.45	4.32
	78	1.03	13.41	9.10	2.04	7.84

The subscript “i” indicates values simulated at the time of satellite overpass

**Table 3.9** Coefficients of variation for METRIC model to estimate actual evapotranspiration (ETa) and crop coefficients (Kc) of a super-intensive drip-irrigated olive orchard. The degrees of freedom (n)= 23123 pixels.

Season	DOY	ETa (%)	Kc (%)
2012-2013	364	8.54	8.54
	30	13.11	13.11
	46	9.91	9.91
	62	9.24	9.24
	78	13.36	13.36

### 3.3 Spatial Variability of Energy Balance Components, ETa, and Kc

Maps indicating the spatial and temporal variability of NDVI, energy balance components (Rni, Gi, Hi and LEi) and olive water requirements (ETa and Kc are illustrated in Figure 3.4, 3.5 and 3.6 for the 2012/2013 growing season, respectively. Figure 3.4 indicates that the tree canopy was relatively uniform during the season and within the olive orchard with a coefficient of variation (CV) ranging between 3.80-7.84% from December 2012 to March 2013. In addition, the intra-orchard spatial variability of Rni (Figure 3.5a-e), Gi (Figure 3.5f-j), Hi (Figure 3.5k-o), and LEi (Figure 3.5p-t) was quite homogeneous with coefficients of variation (CV) less than 15% (Table 3.8). However, the temporal variability was significant with daily mean values within the field Rni, Gi, Hi, and LEi ranging between 452 W m<sup>-2</sup>-642 W m<sup>-2</sup>, 79 W m<sup>-2</sup>-134 W m<sup>-2</sup>, 205 W m<sup>-2</sup>-368 W m<sup>-2</sup>, and 122 W m<sup>-2</sup>-167 W m<sup>-2</sup>, respectively.

In addition, Table 3.9 indicates that the intra-orchard spatial variability of ETa and Kc was not significant with CV ranging between 8.54 and 13.36. Finally, the temporal variability was significant with daily mean values of ET and Kc ranging between 2.09 mm day<sup>-1</sup>-2.89 mm day<sup>-1</sup> and 0.31-0.48, with an n of 23123 pixels.. The value of Kc and ETa has the same CV because in Eq. 1.15 states that the daily reference of evapotranspiration are a single value for the entire field.

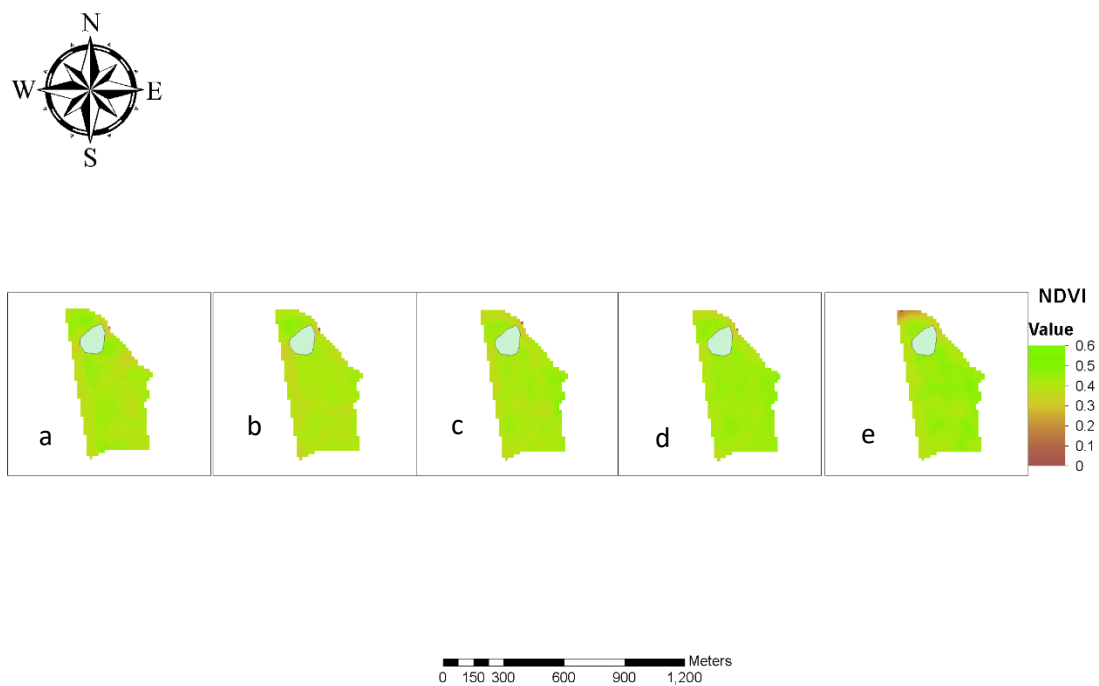


**Figure 3.4.** Temporal and intra-orchard spatial variability of normalized difference vegetation index (NDVI) for a super-intensive drip-irrigated olive orchard during the 2012-2013 growing season. (a), (b),(c), (d) and (e) are maps for DOY 364, 30, 46, 62, and 78, respectively. The area in light blue represent the footprint.

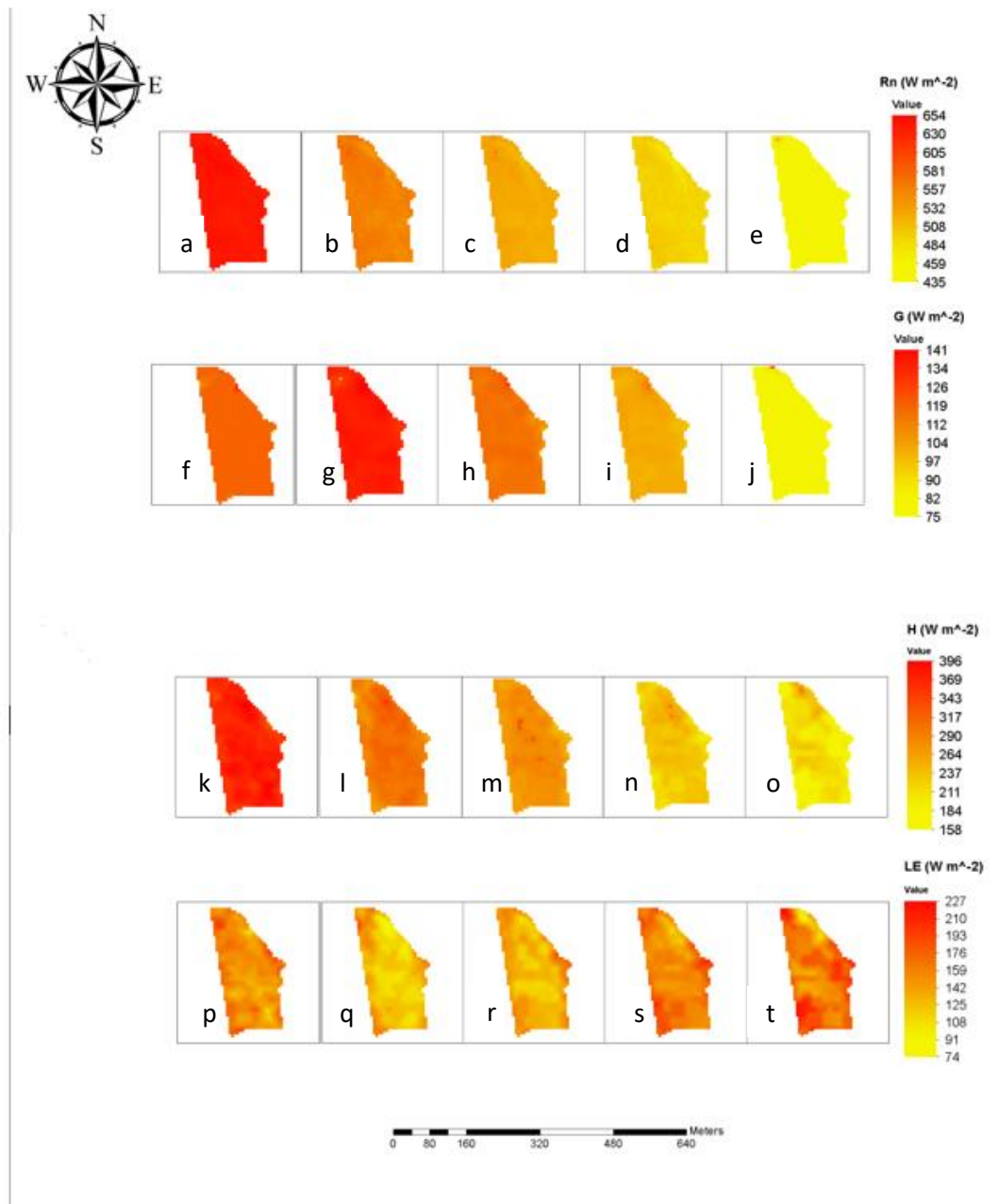


**Figure 3.5.** Temporal and intra-orchard spatial variability of net radiation (Rni), soil heat flux (Gi), sensible heat flux (Hi), and latent heat flux (LEi) over a super-intensive drip-irrigated olive orchard during the 2012-2013 growing season. (a), (f),(k), and (p) are maps for DOY 364, 2012; (b),(g),(l), and (q) are maps for DOY 30, 2013;(c),(h),(m), and (r) are maps for DOY 46, 2013; (d),(i),(n), and (s) are maps for DOY 62, 2013 and (e),(j),(o), and (t) are maps for DOY 78, 2013

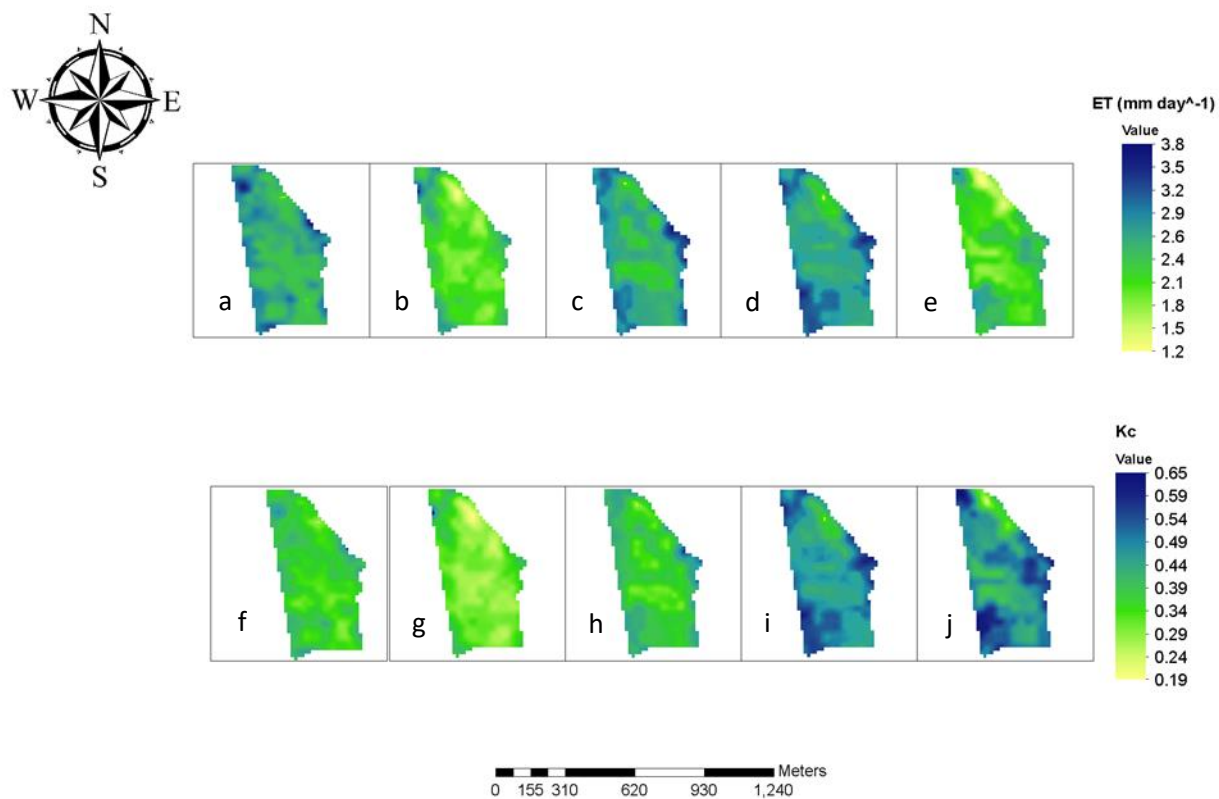


**Figure 3.6.** Temporal and intra-orchard spatial variability of actual evapotranspiration (ETa, mm day<sup>-1</sup>) and crop coefficient (Kc) for a super-intensive drip-irrigated olive orchard during the 2012-2013 growing season. (a) and (f) for maps for DOY 364, 2012; (b) and (g) are maps for DOY 30, 2013; (c) and (h) are maps for DOY 46, 2013; (d) and (i) are maps for DOY 62, 2013 and (e) and (j) are maps for DOY 78, 2013 .

### 3.4 Final Remarks

The results of this study indicate that the performance of METRIC model using the olive-specific functions of LAI, roughness length ( $z_{om}$ ) and G was adequate to simulate energy balance and water requirements on a pixel-by-pixel basis for a super-intensive drip-irrigated olive orchard. It is important to indicate that the canopy size of the olive orchard was maintained almost constant during the study with values of  $f_c$  ranging between 0.2–0.25 and olive trees were maintained under non-water stress conditions ( $\psi_x > -1.5$  MPa). However, commercial olive orchards possess different training systems, tree water status, and canopy sizes, which make the soil-vegetation-atmosphere interaction processes more complicated (Jin et al., 2018). López-Olivarí et al. (2016) indicated that the canopy architecture (tree density, canopy size, LAI, and  $f_c$ ) and training system have an important effect on the partitioning of  $R_n$  inside an orchard and in the distribution of the energy balance components over the land surface. For drip-irrigated orchards with low values of  $f_c$ , the sensible heat flux generated at the soil surface can be a major contributor to the energy balance playing a key role in estimation of LE.



## CHAPTER 4 CONCLUSION

The equations proposed on the literature (Fuentes-Peñailillo et al., 2018; Santos et al., 2012) for METRIC algorithm were suitable to produce an adequate set of maps of  $R_n$ ,  $G$ ,  $H$ ,  $LE$ ,  $ET_a$ , and  $K_c$  for a super-intensive olives orchards in the study field. The positive results between the estimated and observed values that were shown by those fluxes made the maps creation possible. These positive results were, thus, obtained from a parametrized METRIC using the equation provided in literature over a dense hedgerow olive orchard. This modification to METRIC refers to two sources: 1) The equation of  $G$  provide by Fuentes-Peñailillo et al., 2018) ; 2) the model of the Perrier equation on the computation of the momentum roughness length from the crop LAI and height. Although, the error range produced on the energy balance fluxes fluctuated within the range shown in the researched literature. The main source of measuring errors between ground and model calibrated data is associated to  $H$ , also in regards to the selection of hot and cold pixels. In addition, the error of the METRIC parametrization and errors of ground data observation and model calibration.

The results obtained from this research are appropriate for creating a  $K_c$  curve for the different phenological stages using METRIC over an olive orchard.

## References

- Ahumada-Orellana, L.E., Ortega-Farías, S., Searles, P.S., 2018. Olive oil quality response to irrigation cut-off strategies in a super-high density orchard. *Agric. Water Manag.* 202, 81–88. <https://doi.org/10.1016/j.agwat.2018.02.008>
- Ahumada-Orellana, L.E., Ortega-Farías, S., Searles, P.S., Retamales, J.B., 2017. Yield and Water Productivity Responses to Irrigation Cut-off Strategies after Fruit Set Using Stem Water Potential Thresholds in a Super-High Density Olive Orchard. *Front. Plant Sci.* 8, 1280. <https://doi.org/10.3389/fpls.2017.01280>
- Allen, R., Irmak, A., Trezza, R., Hendrickx, J.M.H., Bastiaanssen, W., Kjaersgaard, J., 2011. Satellite-based ET estimation in agriculture using SEBAL and METRIC. *Hydrol. Process.* 25, 4011–4027. <https://doi.org/10.1002/hyp.8408>
- Allen, R., Trezza, R., Tasumi, M., Kjaersgaard, J., 2012. METRIC Mapping Evapotranspiration at High Resolution using Internalized Calibration. *Applications Manual for Landsat Satellite Imagery*. University of Idaho, Kimberly, Idaho.
- Allen, R., Trezza, R., Tasumi, M., Kjaersgaard, J., 2010. METRIC Mapping Evapotranspiration at High Resolution using Internalized Calibration. *Applications Manual for Landsat Satellite Imagery*. University of Idaho, Kimberly, Idaho.
- Allen, R., Walter, I., Elliot, R., Howell, T., Itenfisu, D., Jensen, M., Snyder, R., 2005. The ASCE standardized reference evapotranspiration equation, in: Reston, VA: American Society of Civil Engineers. p. 59.
- Allen, R.G., Pereira, L.S., Raes, D., Smith, M., 1998. Crop evapotranspiration - Guidelines for computing crop water requirements - FAO Irrigation and drainage paper 56, Irrigation and Drainage. FAO.
- Allen, R.G., Tasumi, M., Morse, A., Trezza, R., Wright, J.L., Bastiaanssen, W., Kramber, W., Lorite, I., Robison, C.W., 2007a. Satellite-Based Energy Balance for Mapping Evapotranspiration with Internalized Calibration (METRIC)—Applications. *J. Irrig. Drain. Eng.* 133, 395–406. [https://doi.org/10.1061/\(ASCE\)0733-9437\(2007\)133:4\(395\)](https://doi.org/10.1061/(ASCE)0733-9437(2007)133:4(395))
- Allen, R.G., Tasumi, M., Trezza, R., 2007b. Satellite-Based Energy Balance for Mapping Evapotranspiration with Internalized Calibration (METRIC)—Model. *J. Irrig. Drain. Eng.* 133, 380–394. [https://doi.org/10.1061/\(ASCE\)0733-9437\(2007\)133:4\(380\)](https://doi.org/10.1061/(ASCE)0733-9437(2007)133:4(380))
- Basso, B., Cammarano, D., De Vita, P., 2004. Remotely sensed vegetation indices: theory and application for crop management. *Riv. Ital. di Agrometeorol.* 1, 36–53.
- Bastiaanssen, W.G.M., Menenti, M., Feddes, R.A., Holtslag, A.A.M., 1998. A remote sensing surface energy balance algorithm for land (SEBAL). 1. Formulation. *J. Hydrol.* 212–213, 198–212. [https://doi.org/10.1016/S0022-1694\(98\)00253-4](https://doi.org/10.1016/S0022-1694(98)00253-4)
- Bastiaanssen, W G M, Pelgrum, H., Wang, J., Ma, Y., Moreno, J.F., Roerink, G.J., van der Wal, T., 1998. A remote sensing surface energy balance algorithm for land (SEBAL).: Part 2: Validation. *J. Hydrol.* 212–213, 213–229.

[https://doi.org/https://doi.org/10.1016/S0022-1694\(98\)00254-6](https://doi.org/https://doi.org/10.1016/S0022-1694(98)00254-6)

- Cammalleri, C., Ciraolo, G., Minacapilli, M., Rallo, G., 2013. Evapotranspiration from an Olive Orchard using Remote Sensing-Based Dual Crop Coefficient Approach. *Water Resour. Manag.* 27, 4877–4895. <https://doi.org/10.1007/s11269-013-0444-7>
- Carrasco-Benavides, M., Ortega-Farías, S., Lagos, L.O., Kleissl, J., Morales-Salinas, L., Kilic, A., 2014. Parameterization of the Satellite-Based Model (METRIC) for the Estimation of Instantaneous Surface Energy Balance Components over a Drip-Irrigated Vineyard. *Remote Sens.* 6, 11342–11371. <https://doi.org/10.3390/rs6111342>
- Carrasco-Benavides, M., Ortega-Farías, S., Lagos, L.O., Kleissl, J., Morales, L., Poblete-Echeverría, C., Allen, R.G., 2012. Crop coefficients and actual evapotranspiration of a drip-irrigated Merlot vineyard using multispectral satellite images. *Irrig. Sci.* 1–13. <https://doi.org/10.1007/s00271-012-0379-4>
- Chen, J., Zhu, X., Vogelmann, J.E., Gao, F., Jin, S., 2011. A simple and effective method for filling gaps in Landsat ETM+ SLC-off images. *Remote Sens. Environ.* 115, 1053–1064. <https://doi.org/10.1016/J.RSE.2010.12.010>
- D. Colaizzi, P., R. Evett, S., A. Howell, T., A. Tolk, J., 2006. Comparison of Five Models to Scale Daily Evapotranspiration from One-Time-of-Day Measurements. *Trans. ASABE* 49, 1409–1417. <https://doi.org/https://doi.org/10.13031/2013.22056>
- de la Fuente-Sáiz, D., Ortega-Farías, S., Fonseca, D., Ortega-Salazar, S., Kilic, A., Allen, R., 2017. Calibration of METRIC Model to Estimate Energy Balance over a Drip-Irrigated Apple Orchard. *Remote Sens.* 9, 670. <https://doi.org/10.3390/rs9070670>
- Er-Raki, S., Chehbouni, A., Boulet, G., Williams, D.G., 2010. Using the dual approach of FAO-56 for partitioning ET into soil and plant components for olive orchards in a semi-arid region. *Agric. Water Manag.* 97, 1769–1778. <https://doi.org/https://doi.org/10.1016/j.agwat.2010.06.009>
- Er-Raki, S., Chehbouni, A., Hoedjes, J., Ezzahar, J., Duchemin, B., Jacob, F., 2008. Improvement of FAO-56 method for olive orchards through sequential assimilation of thermal infrared-based estimates of ET. *Agric. Water Manag.* 95, 309–321. <https://doi.org/https://doi.org/10.1016/j.agwat.2007.10.013>
- Ezzahar, J., Hoedjes, J., Er-Raki, S., Chehbouni, A., Boulet, G., Bonnefond, J., de Bruin, H., 2007. The use of the scintillation technique for monitoring seasonal water consumption of olive orchards in a semi-arid region. *Agric. Water Manag.* 89, 173–184. <https://doi.org/10.1016/j.agwat.2006.12.015>
- Foken, T., 2008. THE ENERGY BALANCE CLOSURE PROBLEM: AN OVERVIEW. *Ecol. Appl.* 18, 1351–1367. <https://doi.org/10.1890/06-0922.1>
- Folhes MT, Renno CD, Soares JV (2009) Remote sensing for irrigation water management in the semi-arid Northeast of Brazil. *Agric Water Manag* 96(10):1398–1408. <https://doi.org/10.1016/j.agwat.2009.04.021>

- Fuentes-Peñailillo, F., Ortega-Farías, S., Acevedo-Opazo, C., Fonseca-Luengo, D., 2018. Implementation of a Two-Source Model for Estimating the Spatial Variability of Olive Evapotranspiration Using Satellite Images and Ground-Based Climate Data. *Water* 10, 339. <https://doi.org/10.3390/w10030339>
- Gowda, P., Chavez, J., Colaizzi, P., Evett, S., Howell, T., Tolk, J., 2008. ET mapping for agricultural water management: present status and challenges. *Irrig. Sci.* 26, 223–237.
- Jin, Y., He, R., Marino, G., Whiting, M., Kent, E., Sanden, B.L., Culumber, M., Ferguson, L., Little, C., Grattan, S., Paw U, K.T., Lagos, L.O., Snyder, R.L., Zaccaria, D., 2018. Spatially variable evapotranspiration over salt affected pistachio orchards analyzed with satellite remote sensing estimates. *Agric. For. Meteorol.* 262, 178–191. <https://doi.org/10.1016/j.agrformet.2018.07.004>
- Kalma, J.D., McVicar, T.R., McCabe, M.F., 2008. Estimating Land Surface Evaporation: A Review of Methods Using Remotely Sensed Surface Temperature Data. *Surv. Geophys.* 29, 421–469. <https://doi.org/10.1007/s10712-008-9037-z>
- Kjaersgaard, J.H., Cuenca, R.H., Martínez-Cob, a., Gavilán, P., Plauborg, F., Mollerup, M., Hansen, S., 2009. Comparison of the performance of net radiation calculation models. *Theor. Appl. Climatol.* 98, 57–66. <https://doi.org/10.1007/s00704-008-0091-8>
- Kljun, N., Calanca, P., Rotach, M.W., Schmid, H.P., 2015. A simple two-dimensional parameterisation for Flux Footprint Prediction (FFP). *Geosci. Model Dev.* 8, 3695–3713. <https://doi.org/10.5194/gmd-8-3695-2015>
- Lee, X., Black, T.A., 1993. Atmospheric turbulence within and above a douglas-fir stand. Part II: Eddy fluxes of sensible heat and water vapour. *Boundary-Layer Meteorol.* 64, 369–389. <https://doi.org/10.1007/BF00711706>
- Leuning, R., van Gorsel, E., Massman, W.J., Isaac, P.R., 2012. Reflections on the surface energy imbalance problem. *Agric. For. Meteorol.* 156, 65–74. <https://doi.org/https://doi.org/10.1016/j.agrformet.2011.12.002>
- López-Olivari, R., Ortega-Farías, S., Poblete-Echeverría, C., 2016. Partitioning of net radiation and evapotranspiration over a superintensive drip-irrigated olive orchard. *Irrig. Sci.* 34, 17–31. <https://doi.org/10.1007/s00271-015-0484-2>
- Martínez-Cob, A., Faci, J.M., 2010. Evapotranspiration of an hedge-pruned olive orchard in a semiarid area of NE Spain. *Agric. Water Manag.* 97, 410–418. <https://doi.org/10.1016/J.AGWAT.2009.10.013>
- Ortega-Farías, S., Irmak, S., Cuenca, R.H., 2009. Special issue on evapotranspiration measurement and modeling. *Irrig. Sci.* 28, 1. <https://doi.org/10.1007/s00271-009-0184-x>
- Ortega-Farías, S., López-Olivari, R., 2012. Validation of a two-layer model to estimate latent heat flux and evapotranspiration in a drip-irrigated olive orchard. *Am. Soc.*

- Agric. Biol. Eng. 55, 1169–1178.
- Ortega-Farías, S., Ortega-Salazar, S., Poblete, T., Kilic, A., Allen, R., Poblete-Echeverría, C., Ahumada-Orellana, L., Zuñiga, M., Sepúlveda, D., Ortega-Farías, S., Ortega-Salazar, S., Poblete, T., Kilic, A., Allen, R., Poblete-Echeverría, C., Ahumada-Orellana, L., Zuñiga, M., Sepúlveda, D., 2016. Estimation of Energy Balance Components over a Drip-Irrigated Olive Orchard Using Thermal and Multispectral Cameras Placed on a Helicopter-Based Unmanned Aerial Vehicle (UAV). *Remote Sens.* 8, 638. <https://doi.org/10.3390/rs8080638>
- Ortega-Farías, S., Poblete-Echeverría, C., Brisson, N., 2010. Parameterization of a two-layer model for estimating vineyard evapotranspiration using meteorological measurements. *Agric. For. Meteorol.* 150, 276–286. <https://doi.org/10.1016/j.agrformet.2009.11.012>
- Paço, T.A., Pôças, I., Cunha, M., Silvestre, J.C., Santos, F.L., Paredes, P., Pereira, L.S., 2014. Evapotranspiration and crop coefficients for a super intensive olive orchard. An application of SIMDualKc and METRIC models using ground and satellite observations. *J. Hydrol.* 519, 2067–2080. <https://doi.org/10.1016/J.JHYDROL.2014.09.075>
- Pôças, I., Paço, T.A., Cunha, M., Andrade, J.A., Silvestre, J., Sousa, A., Santos, F.L., Pereira, L.S., Allen, R.G., 2014. Satellite-based evapotranspiration of a super-intensive olive orchard: Application of METRIC algorithms. *Biosyst. Eng.* 128, 69–81. <https://doi.org/10.1016/J.BIOSYSTEMSENG.2014.06.019>
- Santos, C., Lorite, I.J., Allen, R.G., Tasumi, M., 2012. Aerodynamic Parameterization of the Satellite-Based Energy Balance (METRIC) Model for ET Estimation in Rainfed Olive Orchards of Andalusia, Spain. *Water Resour. Manag.* 26, 3267–3283. <https://doi.org/10.1007/s11269-012-0071-8>
- Seguin, B., Courault, D., Guérif, M., 1994. Surface temperature and evapotranspiration: Application of local scale methods to regional scales using satellite data. *Remote Sens. Environ.* 49, 287–295. [https://doi.org/10.1016/0034-4257\(94\)90023-X](https://doi.org/10.1016/0034-4257(94)90023-X)
- Shaomin, L., Hu, G., Lu, L., Mao, D., 2007. Estimation of Regional Evapotranspiration by TM/ETM+ Data over Heterogeneous Surfaces. *Photogramm. Eng. Remote Sensing* 73, 1169–1178. <https://doi.org/10.14358/PERS.73.10.1169>.
- Tasumi M. 2003. Progress in operational estimation of regional evapotranspiration using satellite imagery. Ph.D., University of Idaho, Idaho, USA
- Tasumi, M., Allen, R.G., Trezza, R., 2008. At-Surface Reflectance and Albedo from Satellite for Operational Calculation of Land Surface Energy Balance 51–63.
- Tasumi, M., Allen, R.G., Trezza, R., Wright, J.L., 2005. Satellite-Based Energy Balance to Assess Within-Population Variance of Crop Coefficient Curves. *J. Irrig. Drain. Eng.* 131, 94–109. [https://doi.org/10.1061/\(ASCE\)0733-9437\(2005\)131:1\(94\)](https://doi.org/10.1061/(ASCE)0733-9437(2005)131:1(94))
- Testi, L., Orgaz, F., Villalobos, F.J., 2006. Variations in bulk canopy conductance of an irrigated olive (*Olea europaea* L.) orchard. *Environ. Exp. Bot.* 55, 15–28.

<https://doi.org/10.1016/J.ENVEXPBOT.2004.09.008>

- Testi, L., Villalobos, F., Orgaz, F., 2004. Evapotranspiration of a young irrigated olive orchard in southern Spain. *Agric. For. Meteorol.* 121, 1–18.  
<https://doi.org/10.1016/j.agrformet.2003.08.005>
- Trezza, R., 2006. Evapotranspiration from a remote sensing model for water management in an irrigation system in Venezuela. *Interciencia* 6, 417–423.
- Twine, T.E., Kustas, W.P., Norman, J.M., Cook, D.R., Houser, P.R., Meyers, T.P., Prueger, J.H., Starks, P.J., Wesely, M.L., 2000. Correcting eddy-covariance flux underestimates over a grassland. *Agric. For. Meteorol.* 103, 279–300.  
[https://doi.org/10.1016/S0168-1923\(00\)00123-4](https://doi.org/10.1016/S0168-1923(00)00123-4)
- USGS Global Visualization Viewer [WWW Document], n.d. URL <http://glovis.usgs.gov/> (accessed 2.20.13).
- Villalobos, F., Orgaz, F., Testi, L., Fereres, E., 2000. Measurement and modeling of evapotranspiration of olive (*Olea europaea* L.) orchards. *Eur. J. Agron.* 13, 155–163.  
[https://doi.org/10.1016/S1161-0301\(00\)00071-X](https://doi.org/10.1016/S1161-0301(00)00071-X)
- Williams, D.G., Cable, W., Hultine, K., Hoedjes, J.C.B., Yepez, E.A., Simonneaux, V., Er-Raki, S., Boulet, G., de Bruin, H.A.R., Chehbouni, A., Hartogensis, O.K., Timouk, F., 2004. Evapotranspiration components determined by stable isotope, sap flow and eddy covariance techniques. *Agric. For. Meteorol.* 125, 241–258.  
<https://doi.org/10.1016/J.AGRFORMET.2004.04.008>
- Wilson, K., Goldstein, A., Falge, E., Aubinet, M., Baldocchi, D., Berbigier, P., Bernhofer, C., Ceulemans, R., Dolman, H., Field, C., Grelle, A., Ibrom, A., Law, B.E., Kowalski, A., Meyers, T., Moncrieff, J., Monson, R., Oechel, W., Tenhunen, J., Valentini, R., Verma, S., 2002. Energy balance closure at FLUXNET sites. *Agric. For. Meteorol.* 113, 223–243. [https://doi.org/10.1016/S0168-1923\(02\)00109-0](https://doi.org/10.1016/S0168-1923(02)00109-0)

# TABLE OF CONTENT

	PAGE
CHAPTER 1 INTRODUCTION	1
1.1 Theory	4
CHAPTER 2 MATERIALS AND METHODS	10
2.1 Study Field	10
2.2 Irrigation management and plant measurements	10
2.3 Energy balance measurements	12
2.4 Data quality control	17
2.5 Satellite images	18
2.6 Images processing	19
2.6.1 Functions from literature	19
2.6.2 MATLAB code	20
2.7 Statistical validation	21
CHAPTER 3 RESULTS AND DISCUSSION	23
3.1 Climatic conditions and energy balance ratios	23
3.2 Comparison between Measured and Estimated Variables	26
3.2.1 Evaluation of sub model to estimate soil heat flux	26
3.2.2 Comparison between the different fluxes	27
3.3 Spatial Variability of Energy Balance Components, ETa and Kc	33

3.4 Final Remarks	37
CHAPTER 4 CONCLUSION	38
References	39



## LISTS OF MULTIMEDIA OBJECTS

Equation			Page
<b>Eq 1.1</b>	$LE_i$		2
<b>Eq. 1.2</b>	$Rn_i$		4
<b>Eq. 1.3</b>	$\alpha$		4
<b>Eq. 1.4</b>	$\frac{G_i}{Rn_i}$	if $LAI \geq 0.5$	5
		Allen et al., 2010	
<b>Eq. 1.5</b>	$\frac{G_i}{Rn_i}$	if $LAI < 0.5$	5
		Allen et al., 2010	
<b>Eq. 1.6</b>	$\frac{G_i}{Rn_i}$		5
		Allen et al., 2010	
<b>Eq. 1.7</b>	$\frac{G_i}{Rn_i}$		5
		Allen et al., 2012	
<b>Eq. 1.8</b>	$LAI$	for $SAVI \leq 0.817$	6
<b>Eq. 1.9</b>	$LAI$	for $SAVI > 0.817$	6
<b>Eq. 1.10</b>	$H_i$		6
<b>Eq. 1.11</b>	$Z_{om}$		6
<b>Eq. 1.12</b>	$\Delta T_s$		6
<b>Eq. 1.13</b>	$H_{cold}$		7
<b>Eq. 1.14</b>	$ETa_i$		8
<b>Eq. 1.15</b>	$ETa$		8
<b>Eq. 1.16</b>	$ET_{rF}$		8
<b>Eq. 1.17</b>	$ET_{r24}$		9
<b>Eq. 1.18</b>	$ET_{rh}$		9

<b>Eq. 2.1</b>	G	15
<b>Eq. 2.2</b>	S	15
<b>Eq. 2.3</b>	G	16
<b>Eq. 2.4</b>	$LE_{BR}$	17
<b>Eq. 2.5</b>	$ET_{BR}$	17
<b>Eq. 2.6</b>	LAI	19
<b>Eq. 2.7</b>	$z_{om}$	19
<b>Eq. 2.8</b>	G	20
<b>Eq. 2.9</b>	$\frac{G_i}{Rn_i}$	20
<b>Eq. 2.10</b>	$\frac{G_i}{Rn_i}$	20
<b>Eq. 2.11</b>	RMSE	22
<b>Eq. 2.12</b>	MAE	22
<b>Eq. 2.13</b>	$I_a$	22

Tables	Page
<b>Table 2.1.</b> Images selected for processing surface energy balances over a drip-irrigated olive orchard with their percentage cloud covering	18
<b>Table 3.1.</b> Mean daily values of air temperature ( $T_a$ ), vapor pressure deficit (VPD), wind speed ( $u$ ) and wind direction ( $w$ ) at the time of satellite overpass. Also, daily reference evapotranspiration ( $E_{Tr}$ ) is included.	24
<b>Table 3.2.</b> Energy balance closure (EBC), Bowen ratio ( $\beta$ ) and instantaneous ratios of latent ( $LE\beta$ ), sensible ( $H\beta$ ) and soil ( $G$ ) heat fluxes to net radiation ( $R_n$ ) for a drip-irrigated orchard. Instantaneous ratio of $R_n$ to incoming solar radiation ( $R_s$ ) is also included.	26
<b>Table 3.3.</b> Evaluation of calibrated sub-models to estimate soil heat flux ( $G_i$ ) a super-intensive drip-irrigated olive orchard at the time of satellite overpass.	27
<b>Table 3.4.</b> Validation of sub-models to estimate incoming solar radiation ( $R_{si}$ ), net radiation ( $R_n$ ), sensible heat flux ( $H$ ), soil heat flux ( $G$ ), and latent heat flux ( $LE$ ) of a super-intensive drip-irrigated olive orchard at the time of satellite overpass.	28
<b>Table 3.5.</b> Evapotranspiration ( $ET_a$ ) and crop coefficients ( $K_c$ ) implemented the models from literature over of a super-intensive drip-irrigated olive orchard.	30

**Table 3.6.** Estimates and measured values of incoming solar radiation (Rsi), net radiation (Rn), soil heat flux (G), sensible heat flux (H) y latent heat flux at the time of satellite overpass 31

**Table 3.7** Estimates and measured values of actual evapotranspiration (ETa) and crop coefficient (Kc) at the day of satellite overpass 32

**Table 3.8.** Coefficient of variation of sub-models to compute net radiation (Rn), sensible heat flux (H), soil heat flux (G), and latent heat flux (LE) of a super-intensive drip-irrigated olive orchard. 32

**Table 3.9** Coefficient of variation of METRIC model in estimate actual evapotranspiration (ETa) and crop coefficients (Kc) of a super-intensive drip-irrigated olive orchard 32

Figures	Page
<p><b>Figure 2.1.</b> Experimental site with drip-irrigated olive trees (Quepo, Penciahue Valley, Maule Region, Chile). Whsite dot shows the location of the eddy covariance (EC) system and the arrow represents the typical wind direction towards the EC system at the time of satellite overpasses. The transparent area represents the average footprint area and the light green area was used to sample pixels for validating the METRIC model to estimate energy balace components, evapotranspiration and crop coefficient on a pixel-by-pixel basis.</p>	11
<p><b>Figure 2.2.</b> Experimental site of a drip-irrigated olive orchard (November 2013, Penciahue Valley, Maule Region of Chile)</p>	11
<p><b>Figure 2.3.</b> Analytical footprint model under unstable conditions in terms of relative and cumulative contribution, respectively for the days used in this study.</p>	14
<p><b>Figure 2.4.</b> Eddy Covariance system installed within the experimental site (November 2013, Penciahue Valley, Maule Region of Chile).</p>	15
<p><b>Figure 2.5.</b> Distribution of soil heat flux (G) measurements for a drip-irrigated olive orchard. The positions 1,2,7 and 8 indicated that fluxes were measured between rows while positions 3, 4, 5 and 6 show that fluxes were obtained below the tree canopy (3, 4, 5 and 6). Also, the asterisks and open circles indicate the location of drippers and G measurements, respectively</p>	16
<p><b>Figure 2.6.</b> Flowchart of MATLAB code for image processing</p>	21
<p><b>Figure 3.1.</b> Energy balance closure (EBC) at 30-min</p>	

intervals for days when satellite overpassed during 2011-2012 and 2012-2013 growing season. Days presenting values of  $E_{Bc} < 0.7$  or  $> 1.3$  were excluded from this study to reduce the uncertainty associated with errors in the LE measurements

**Figure 3.2.** Comparisons at the time of satellite overpass between observed (axis X) and estimated (axis Y) values of net radiation (Rn), soil heat flux (G), sensible heat flux (H), latent heat flux (LE), and shortwave incoming radiation (Rsi) from a modified METRIC over a super-intensive drip-irrigated olive orchard. The solid line represents the 1:1 line.

**Figure 3.3.** Daily comparisons between observed (axis X) and estimated (axis Y) values of actual evapotranspiration (ETA) from a modified METRIC of a super-intensive drip-irrigated olive orchard. The solid line represents the 1:1 line.

**Figure 3.4.** Temporal and intra-orchard spatial variability of normalized difference vegetation index (NDVI) for a super-intensive drip-irrigated olive orchard during the 2012-2013 growing season. (a), (b),(c), (d) and (e) are maps for DOY 364, 30, 46, 62, and 78, respectively. The area in light blue represent the footprint.

**Figure 3.5.** Spatial distribution of ET (mm day<sup>-1</sup>) and Kc corresponding to day of the season 2012-2013. (a), and (f) is the DOY 364 of 2012; (b), and (g) is the DOY 30 of 2013; (c), and (h) is the DOY 46 of 2013; (d),and (i) is the DOY 62 of 2013 and (e), and (j) is the DOY 78 of 2013

**Figure 3.6.** Temporal and intra-orchard spatial variability of actual evapotranspiration (ETA, mm day<sup>-1</sup>) and crop coefficient (Kc) for a super-intensive drip-irrigated olive orchard during the 2012-2013 growing season. (a) and (f) for maps for DOY 364, 2012; (b) and (g) are maps for DOY 30, 2013; (c) and (h) are maps for DOY 46, 2013; (d) and (i) are maps for DOY 62, 2013 and (e) and (j) are maps for DOY 78, 2013 .